Moving the heat around: the impact of metamorphism on the distribution of crustal heat production

Thesis submitted in accordance with the requirements of the University of
Adelaide for an Honours Degree in Geology

Christopher Wilde Kemp

November 2014

THE UNIVERSITY
of ADELAIDE

MOVING THE HEAT AROUND: THE IMPACT OF METAMORPHISM ON THE DISTRIBUTION OF CRUSTAL HEAT PRODUCTION

RUNNING TITLE: METAMORPHIC IMPACT ON CRUSTAL HEAT PRODUCTION

ABSTRACT

Crustal differentiation has resulted in the concentration of heat producing elements (HPEs) in the upper crust due to partial melting processes. Recent studies into the mineral hosts of HPEs have shown that it may be possible to enrich a rock in HPEs via partial melting rather than depleting it. This paper details transects that were performed across metamorphic grade at Mt Stafford, the Reynolds Ranges and Broken Hill using portable Gamma Ray Spectrometer (GRS) devices. The paper found that there is a small, but significant rise in heat production with an increase in metamorphic grade from greenschist to granulite facies rocks exposed at the surface at those locations driven by thorium concentration. A definite non-linear trend pattern was also found in the distribution of heat production with increasing grade, predominantly at Mt Stafford. The methods and findings were compared to contemporary airborne radiometry scans and geochemical assay studies at Mt Stafford in order to compare the newer largely untested GRS method to these modern standards. Findings indicate that the HPE bearing rocks at these locations are enriched enough in HPEs that they can further self-enrich in open partial melting systems, increasing heat production and leading to structurally weaker crust.

KEYWORDS

Metamorphism, Crustal heat production, Radiogenic heat production, Distribution of heat production, Portable gamma ray spectrometry, Field sampling, Mt Stafford, Reynolds Ranges, Broken Hill.

TABLE OF CONTENTS

LIST OF FIGURES AND TABLES

1. INTRODUCTION

Heat Producing Element (HPE) bearing minerals within the crystalline upper crust are found at different pressures and temperatures depending on their mineral stability envelopes (Vilà et al. 2010, Yakymchuk and Brown 2014, Graessner and Schenk 2000, Spear 1993). A package of rock that has undergone metamorphism – changes in heat and pressure - will contain the minerals which were stable at the peak pressure and temperature that that rock package reached (Vigneresse et al. 1989, Bea 2012). The common understanding is that depending on the conditions reached during peak metamorphism, the common minerals in which HPEs reside, zircon, monazite, apatite and xenotime may have become part of a partial melt and been transported out of the system, leaving a residual compositionally HPE depleted rock behind. As these minerals break down with increasing pressure and temperature (Kelsey and Powell 2010, Vigneresse et al. 1996, Kelsey et al. 2008), high grade metamorphic rocks such as granulites should be more depleted in HPE minerals than rocks which had not undergone partial melting (Bea 2012, Mareschal and Jaupart 2013). Such behaviour is evident in the general composition of granite plutons near the surface of the crust, which in many cases contain a significant volume of crustal material derived from partial melting. Granites are extremely enriched in HPEs compared to global rock averages (Taylor and McLennan 1995), implying that crustal reservoirs associated with granitic magmatism should then be correspondingly depleted in HPEs.

Large-scale partial melting leading to complete breakdown of HPE bearing minerals monazite and zircon generally requires extreme temperature conditions near the upper limit of ultrahigh temperature metamorphism, at above $900\,^{o}\text{C}$ (Kelsey and Powell

2010, Spear 1993, Taylor and McLennan 1995). However, if the P-T conditions don't reach these extremes instead of granulite facies rocks being depleted in HPEs, they may become enriched compared to their protolith composition. Because of the temperature dependence of zircon and monazite solubility in partial melts (Kelsey and Powell 2010, Yakymchuk and Brown 2014), enrichment could occur if partial melting occurred at comparatively low metamorphic grades, around the transition between upper amphibolite and granulite, resulting in decreasing volume associated with melt loss but with only limited loss of HPEs to the melt, leading to HPE enrichment in the residual material.

There have been relatively few studies that systematically set out to examine the relationship between HPE concentrations and metamorphic grade. A number of workers have examined the way in which HPE concentrations vary with crustal depth (Brady et al. 2006, Ray et al. 2008, Andreoli et al. 2006, Fountain and Rudnick 1995). For example, Fountain (1995), determined HPE concentrations in obliquely exposed crustal sections in the North American Shield, finding that lower crustal sections had a lower degree of heat production. Similarly Ray *et al.* (2008) examined crustal sections in the Indian Shield and Andreoli (2006) looked at granulites within the Western Namaqualand Belt of South Africa, both finding enriched granulites in the lower crust. Other studies (McLaren et al. 2003, Gazzaz and Hashad 1991, Ashwal et al. 1987, Kumar et al. 2007, Vigneresse et al. 1989), generally found significantly reduced HPE concentrations in the deeper sections of crust. In most cases, this reduction in HPE concentration coincided with a major change in rock type, which generally reflected older igneous dominated basement that was compositionally unrelated to the rock

systems higher in the crust. Therefore these studies did not directly determine the impact that metamorphism has on modifying the HPE concentrations of a traceable protolith.

This paper aims to present data on the concentration and distribution of the heat producing elements uranium, thorium and potassium across a number of exposed rock sequences that range from subsolidus to suprasolidus conditions in order to study whether radiogenic heat production increases or decreases as metamorphic grade increases. Along the way, it compares the different methods of determining HPE concentration from outcrop-scale sampling, principally hand-held gamma ray spectrometry and analytical geochemistry. The paper also looks at the differences between outcrop level sampling and airborne derived datasets of the same area. Looking at HPE driven heating of the crust on a global scale is crucial to the understanding of deformation and stability of both the upper and lower crust as this heat generation determines whether the intracontinental crust will act as a stable craton, or deform on a massive scale creating a rift or orogenic belt (Sandiford et al. 2001, Sandiford et al. 2002).

2. GEOLOGICAL SETTING

Three field areas were chosen for this study. Two are located in central Australia; Mt Stafford and the Reynolds Ranges, with the third in the Broken Hill region (Figure 1)
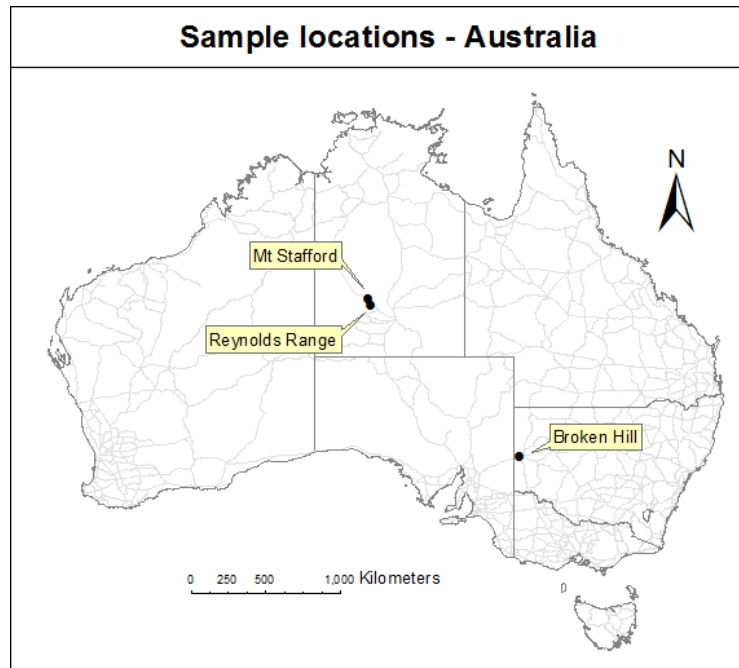
Figure 1: Locations of the field sites

In the following sections, a summary of the geology of each region is provided.

2.1 Mt Stafford

Mt Stafford occurs in the Anmatjira-Reynolds Range area of the Proterozoic Arunta Inlier of Central Australia. The area is dominated by amphibolite to granulite facies metapelites (see Table 1) and large volumes of deformed granitoids (Stewart 1981, Warren 1983) which record a complex polymetamorphic history. The Mt Stafford area is dominated by metamorphosed turbidites of the 1850-1820 Ma Lander Rock Beds, which reached peak metamorphism at around 1800 Ma (Rubatto et al. 2006). The area also preserves a second event with limited effects which occurred around 1600 Ma (Vry et al. 1996, Williams et al. 1996). The area studied consists of interbedded aluminous

metapsammitic and metapelitc layers and cordierite granofel beds on a centimeter to meter scale, a package known as the Mt Stafford Beds (White et al. 2003).

At Mt Stafford, the metamorphism ranges from greenschist to granulite facies over a distance of 10km, consisting of a peak high temperature, low pressure metamorphism at 775-785°C and 3.3 to 4 kbar in the granulite zone (White et al. 2003).

For this study, the isograds presented by White *et al.* (2003) were used as the principal method of sorting the sample sites by metamorphic grade (Figure 2) as it is the most recent paper mapping the isograds in the area, taking into account the extensive past studies of the area by Greenfield *et al.* (White et al. 2003, Greenfield et al. 1996, Greenfield et al. 1998).
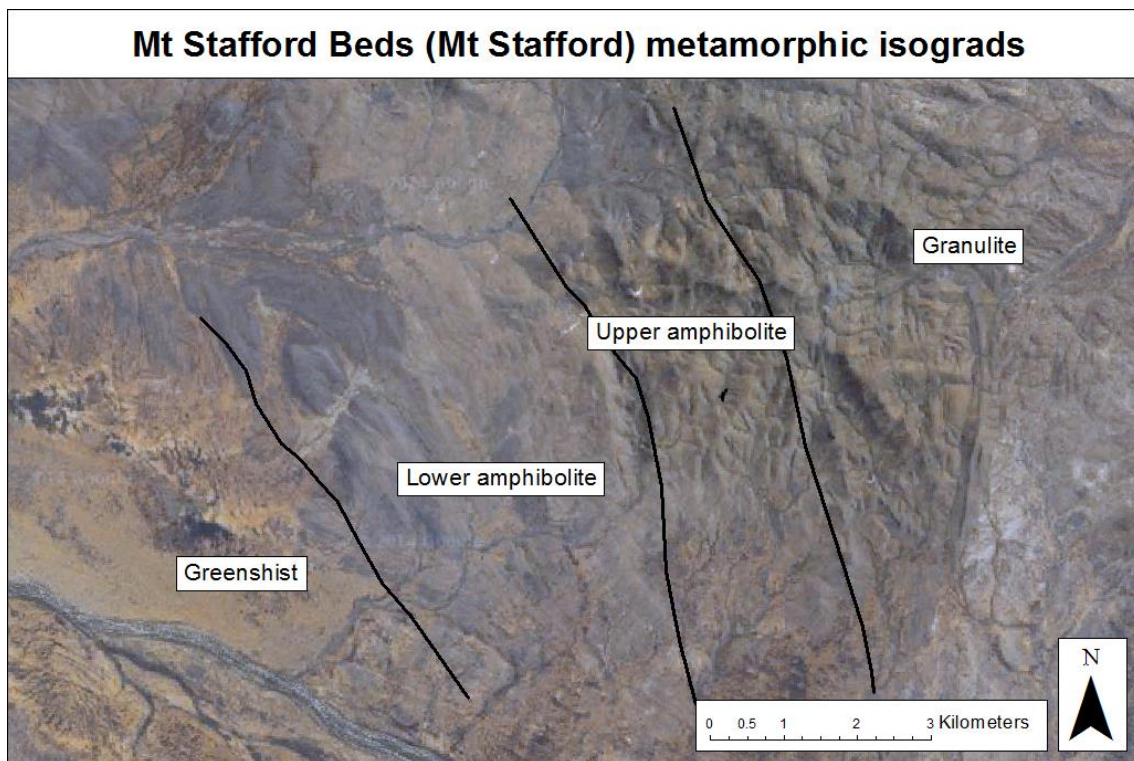
Figure 2: Metamorphic isograds of the Mt Stafford Beds, from (White et al. 2003).

2.2 Broken Hill

The Broken Hill Block comprises Paleoproterozoic metasediments collectively named the Willyama Supergroup. The sediments were deposited in an evolving rift basin (Stevens et al. 1988) between 1.17-1.67 Ga (Page et al. 2000, Page et al. 2005). The basin into which the Willyama Supergroup was deposited was inverted during the Olarian Orogeny c. 1.6-1.59 Ga (Page et al. 2000). The inversion involved high temperature low pressure metamorphism (Hobbs et al. 1984, Stevens et al. 1988), reaching peak amphibolite to granulite facies metamorphism at c. 1.6 Ga (Page and Laing 1992, Forbes et al. 2008). The Willayama Supergroup was then deformed and metamorphosed to greenschist facies during the Delamarian Orogeny at c. 520-490 Ma (Forbes et al. 2005). Peak metamorphism of the Broken Hill rocks was achieved in the Olarian orogeny, when temperatures reached $740^{o}C$ and pressures reached 5 kbar in the granulite zone (Forbes et al. 2005). The Sundown Group was used a traceable protolith for this study because it occurs across the entire metamorphic gradient in the region (Figure 3). It ranges up 1500m thick and is comprised of metamorphosed chemically mature quartz rich sands and shales (Stevens et al. 1988) that were deposited at around 1680 Ma (Page et al. 2005). At the lowest metamorphic grades the rocks consist of andalusite-bearing micaeous assemblages. At granulite grade, metamorphism has resulted in the formation of coarse-garnet bearing migmatitic assemblages.

Broken Hill is one of the best mapped areas in Australia due to the mining in the area and the use as a study site for many papers. For this paper, the isograds from (Webb and Crooks 2005) were used to delineate metamorphic grade (Figure 3).
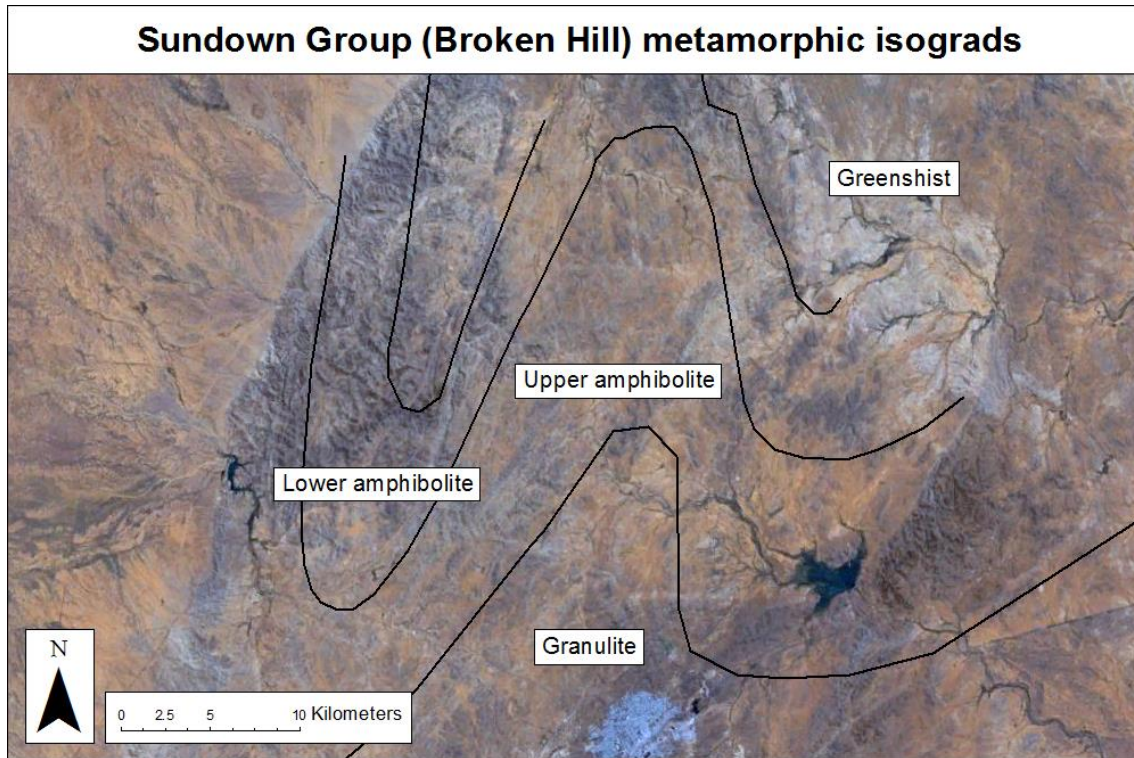
Figure 3: Metamorphic isograds in the Broken Hill area, including the Sundown group. From (Webb and Crooks 2005).

2.3 Reynolds Range

The Reynolds Range area has experienced at least four major tectonothermal events. The first of these was the Stafford Tectonic Event at around 1800 Ma, producing an upright, north trending fabric in the north western Reynolds Range. Following the deposition of the Reynolds Range Group sometime between c. 1806 and 1785 Ma (Hand and Buick 2001), the region was intruded by voluminous sheet-like granites that produced contact metamorphism that may have locally reached granulite (Collins and Shaw 1995). At around 1595 – 1570 Ma, the Chewings Orogeny created widespread metamorphism, ranging from greenschist facies in the north western Reynolds Range to granulite facies in the south east (Hand et al. 1995, Vry et al. 1996, Williams et al. 1996, Collins 2000), (Figure 4). Finally, during the Alice Springs Orogeny, at around 400-300 Ma, the region was dissected by SE-E trending shear zones, which themselves show an

increase in metamorphic grade toward the south east from sub-greenschist to mid amphibolite facies (Hand and Buick 2001, Mawby et al. 1999). Peak metamorphism for the Reynolds Range area occurred during the Chewings Orogeny, where pressure/temperature conditions reached 750-800°C and 5 kbar at the granulite facies zone (Buick et al. 1998). The Pine Hill Formation, comprising shale, slate, siltstone and quartzite and their metamorphic equivalents (see Table 1), is 500 to 600 meters thick (Dirks 1990) and was chosen for this paper as the package outcrops in both the north western greenschist facies region as well as the south eastern granulite region.

The metamorphic isograds for the Reynolds Range were sourced from the paper (Hand and Buick 2001), (Figure 4).
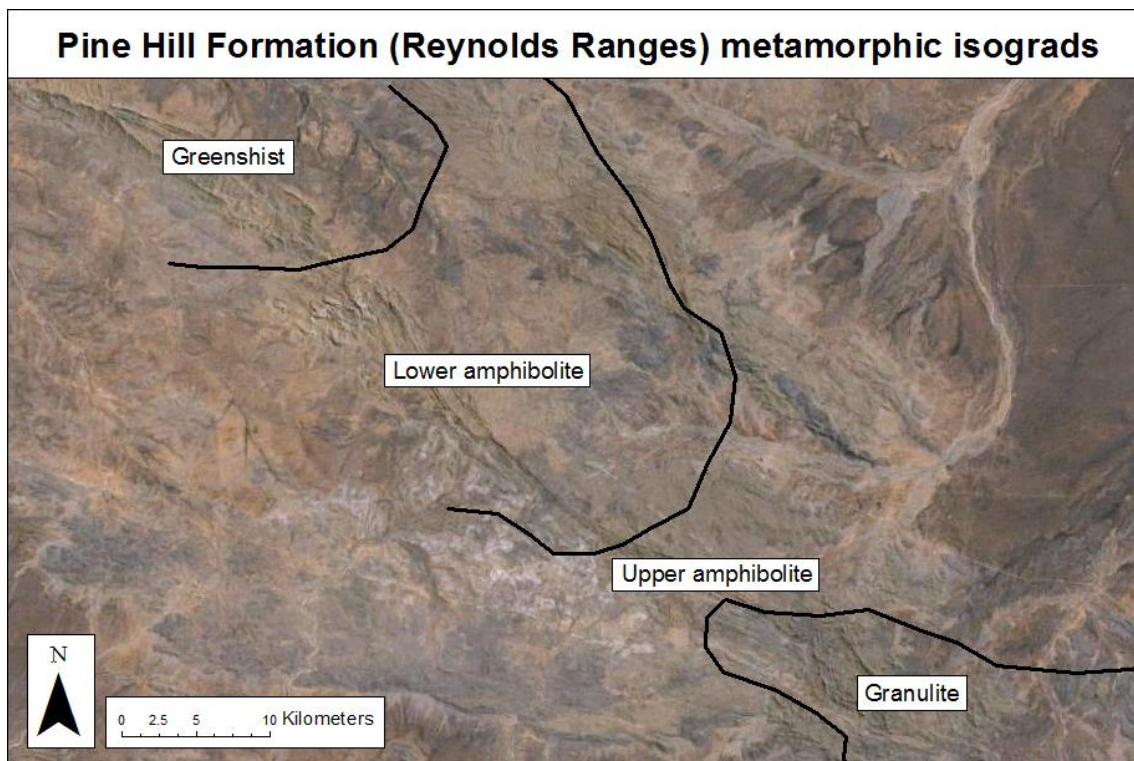
Figure 4: Metamorphic isograds of the Reynolds Range area, including the Pine Hill Formation. From (Hand and Buick 2001).

Greenschist Facies	Amphibolite Facies	Granulite Facies
Mt Stafford Beds, showing the metapelitc (left) and metapsammitic (right) interbedded layers.	Mt Stafford Beds, showing a more homogenous rock with no definite bed layering remaining.	Mt Stafford Beds, garnet-bearing migmatitic assemblage
Broken Hill Sundown Group, metapsammite	Broken Hill Sundown Group, foliation defined by sillimanite-biotite-muscovite.	Broken Hill Sundown Group, containing large crystals of garnet 1-4cm in diameter associated with partial melting
Reynolds Range Group Pine Hill Formation, phyllite.		Reynolds Range Group Pine Hill Formation, showing cordierite crystals ~5-10mm in diameter.

Table 2: Field photos of the nature of the outcrops across metamorphic grade at each of the three field locations. Scales: The GPS unit is about 10 cm long, the pens are around 15 cm long, the portable GRS device in the yellow case is around 30cm tall and the boot is around 13cm across. No locations at amphibolite grade were visited in the Reynolds Range.

3. METHODS

The three field areas all contain a single protolith rock package of greenschist to granulite facies which outcropped extensively. In the case of the Reynolds Range, the contact between the Pine Hill Formation and the underlying Mt Thomas Quartzite can be traced continuously from greenschist to granulite providing a very tight control on the stratigraphic position of the sample sites at different metamorphic grades. In the Broken Hill area, due to the complexity of deformation and locally obscured boundaries with adjacent units, the exact stratigraphic position of sample sites within the Sundown Group is uncertain, however sampling traverses at each location attempted to transect the entire unit. At Mt Stafford, the precise stratigraphic positions of sample locations in the Mt Stafford beds are uncertain. All sample sites comprised metamorphosed interbedded pelitic and pssamopelitic turbidite units.

3.1 Portable gamma ray spectrometer measurements

The raw data was obtained by field measurements at outcrops with portable Gamma Ray Spectrometer (GRS) handheld devices. Four of these GRS devices were used to assay the outcrops for periods of 3 minutes per outcrop, to gain an accurate reading of the quantities of HPEs in close proximity to the device (Figure 5). The four devices were used together to try to eliminate local variations in the outcrop material but also in case there was drift in the readings from any one device.

The portable GRS devices work by detecting passing gamma rays with a large 2 by 2 inch bismuth germanium oxide (BGO) crystal detector and creating a spectrum by plotting the count of gamma rays over the sample period versus their energy. This spectrum plot is then analysed by systems within the device, measuring the number of gamma rays between specific energy levels indicative of the presence of decaying potassium, thorium and uranium and their more active isotopes. This count is then translated by the internal firmware and displayed on the screen on the front of the device as quantity percentages and parts per million of potassium, thorium and uranium.

Figure 5: Portable GRS devices at a sample location at Mt Stafford

The HPE readings from the outcrops from the GRS devices were then used to calculate Radiogenic Heat Production (RHP) in each of the metamorphic sections using the method proposed by Rybach (1988), using a density of 2750g/m^3, the average density of the rock packages studied (Rybach 1988, Christensen and Mooney 1995). At least 8 outcrop sites were chosen in each of the areas of metamorphic grade – greenschist, upper and lower amphibolite and granulite - across the transect between isograds, although due to the distance between isograds and the availability of outcropping material this was increased to over 150 outcrops in some cases.

Specially designed concrete pads at the Geoscience Australia facility in Therbarton, a suburb of Adelaide, were used to calibrate the devices. Each of the pads has known quantities of each of the three HPEs and was used to calibrate the devices and scale them correctly before the devices were taken into the field. This process was undertaken using the instructions provided by the manufacturer in the documentation accompanying the devices (links to manuals given in Appendix 1). The same slabs were also used in checking the readings on the devices when they were returned from the field in order to calculate possible error due to drift over time.

To help to eliminate error in the data, readings were taken on the same outcropping at the start and end of each fieldtrip to find any drift in the instrumentation. In the few cases that were found where the devices were incorrectly reading by a scalar, this quantity was found using the pads and the data corrected by that scalar before data analysis took place. Further verification of the data from the field was also obtained by downloading the data as spectrums from the devices and independent calculation of the concentrations of the elements (See Appendix 1).

Microsoft Excel was used as a database program for the raw data and calculations, with the Excel add on 'Isoplot' (Ludwig 2014) as well as the original graphing applications used to show the relationships within the data. In order to ensure that the samples for each metamorphic section was correctly identified, each of the field areas was mapped using a GIS program – ArcGIS Arcmap 10 - along with metamorphic isograd maps from previous studies of the sample areas.

The GIS overlays created in order to compare the ground-based GRS readings and the airborne radiometry were compiled from separate layers of the uranium, thorium and potassium concentrations using Raybach's formula via the Quantum GIS (QGIS) program, assuming rock densities of $2600g/m^3$ across the field areas (Rybach 1988). The concentration maps were sourced from (Minty et al. 2010). The difference in assumed density between the formula used for the outcrops ($2750g/m^3$) and the airborne data was due to the need to incorporate less dense sedimentary material into the airborne data maps.

3.2 Geochemistry

Samples taken from the transects were analysed for major and selected trace elements. Bulk chemical compositions of samples were determined using whole-rock geochemical analyses. Major element concentrations were determined by X-ray fluorescence (XRF), using a Panalytical 2404 XRF unit at Franklin and Marshall College in the United States. Samples were prepared for analysis by fusion of the milled sample with lithium tetraborate. Trace element samples were prepared for analysis by mixing the milled sample with Copolywax powder.

The Mt Stafford and Reynolds Range geochemical samples were collected in tandem with the GRS transects and so directly reflect the geochemistry of the studied areas. This method allows for a general comparison of geochemical assays and GRS readings as they both sample across metamorphic grade and can be broken down into the same four metamorphic groups: greenschist, lower and upper amphibolite and granulite facies.

3.3 Elemental Mapping

Element maps were created using a SX-5 scanning electron microprobe at Adelaide Microscopy. Elemental detection was done using a 100nA current with 20kV accelerating voltage on a raster function using thin section slides of greenschist and granulite facies rocks from each of the field areas. The 20 by 20 millimetre maps were then used to identify coincident hot spots of calcium-phosphorous (indicating apatite), cerium-phosphorous (indicating monazite), yttrium- phosphorous (indicating xenotime) and zirconium (indicating zircon). The density of hot spots indicating the presence of each mineral were then measured using a program called ImageJ along with a pixel counting tool in order to create a count of the hotspots in each element map. These counts can then be used to infer the changing quantities of the HPE bearing elements zircon, monazite, apatite and xenotime between greenschist and granulite grade rocks at each of the field sites.

4. RESULTS

All three metamorphic sample locations - Mount Stafford, Broken Hill and the
Reynolds Ranges – were successfully sampled using planned representative transects
with a single protolith per field area using the portable GRS systems. The results of
these transects are detailed in figures 6 to 14. All measured U-Th-K data from GRS
determinations are presented in Appendix 3. All geochemical data determined by XRF
are presented in Appendix 4.
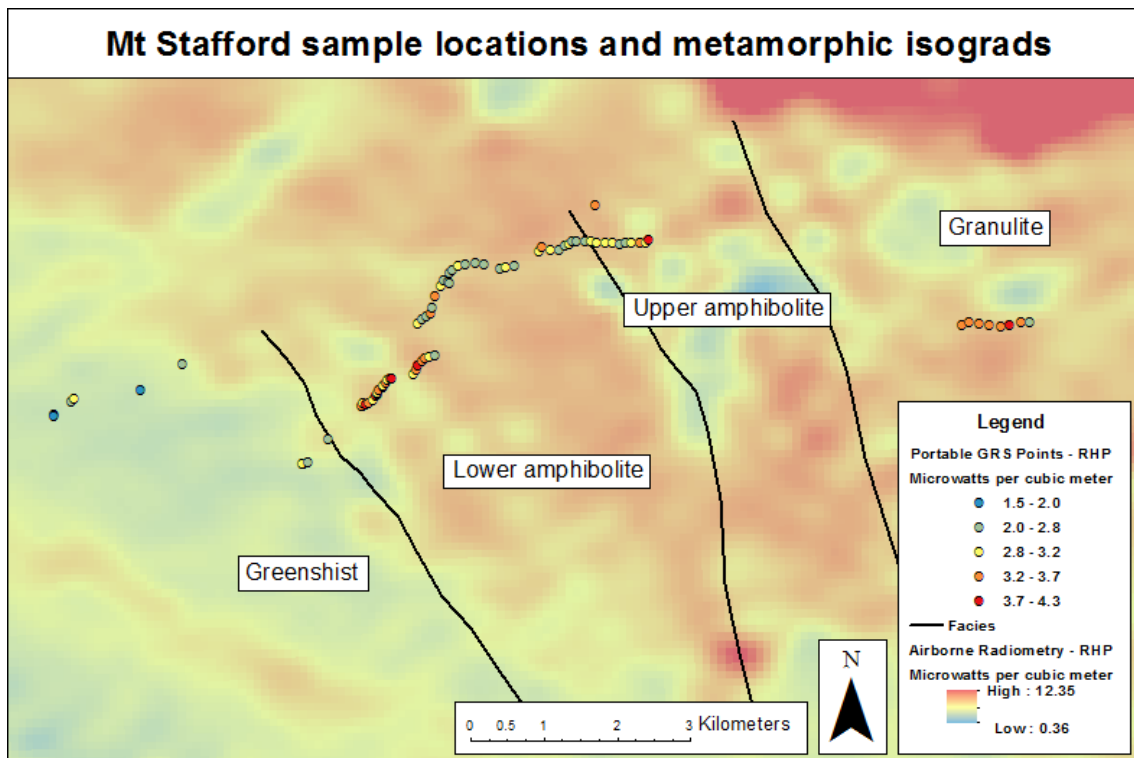
**Figure 6: Locations of the sample sites at Mt Stafford along with their radiogenic heat production
as determined by protable GRS. The raster overlay is RHP calculated from airborne radiometry
was calculated from seperate U, Th and K layers from Geoscience Australia. Both data sets used
the formula from Rybach 1988 to calculate RHP (Rybach 1988). The zones are those defined in the
paper by (White et al. 2003).**
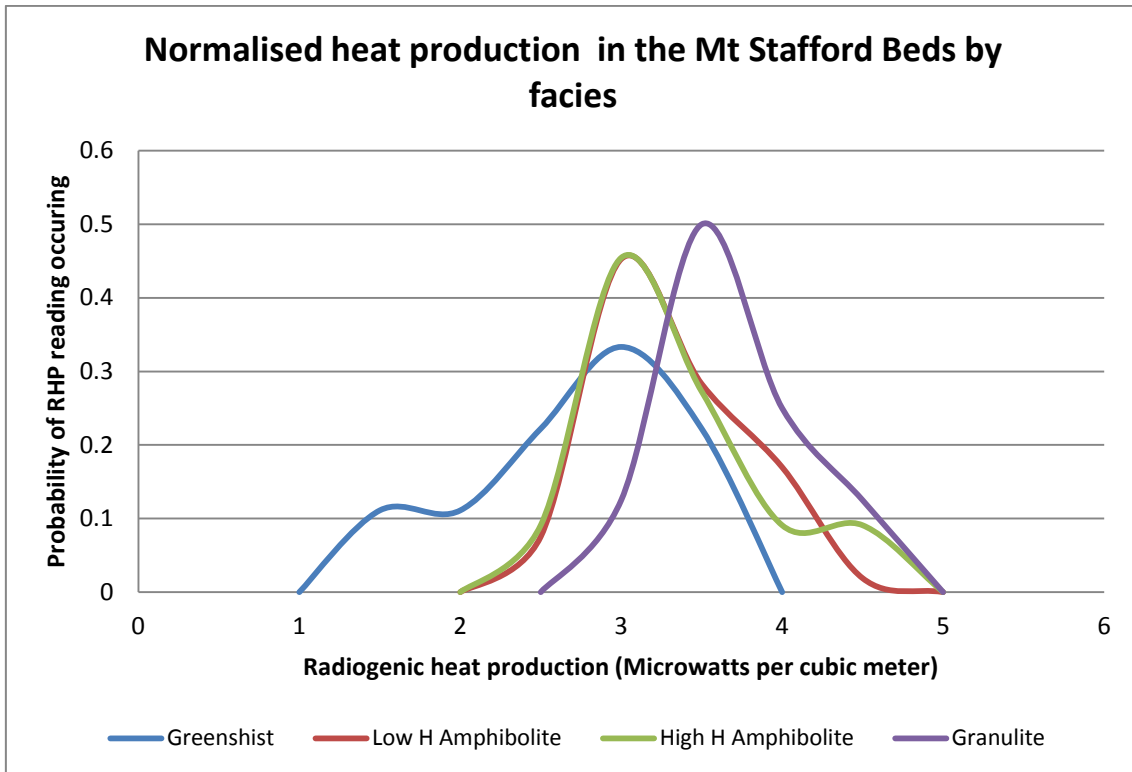
Figure 7: Normalized heat production determined via GRS measurements in each of the metamorphic grades (greenschist, lower and upper amphibolite and granulite) in the Mt Stafford beds.
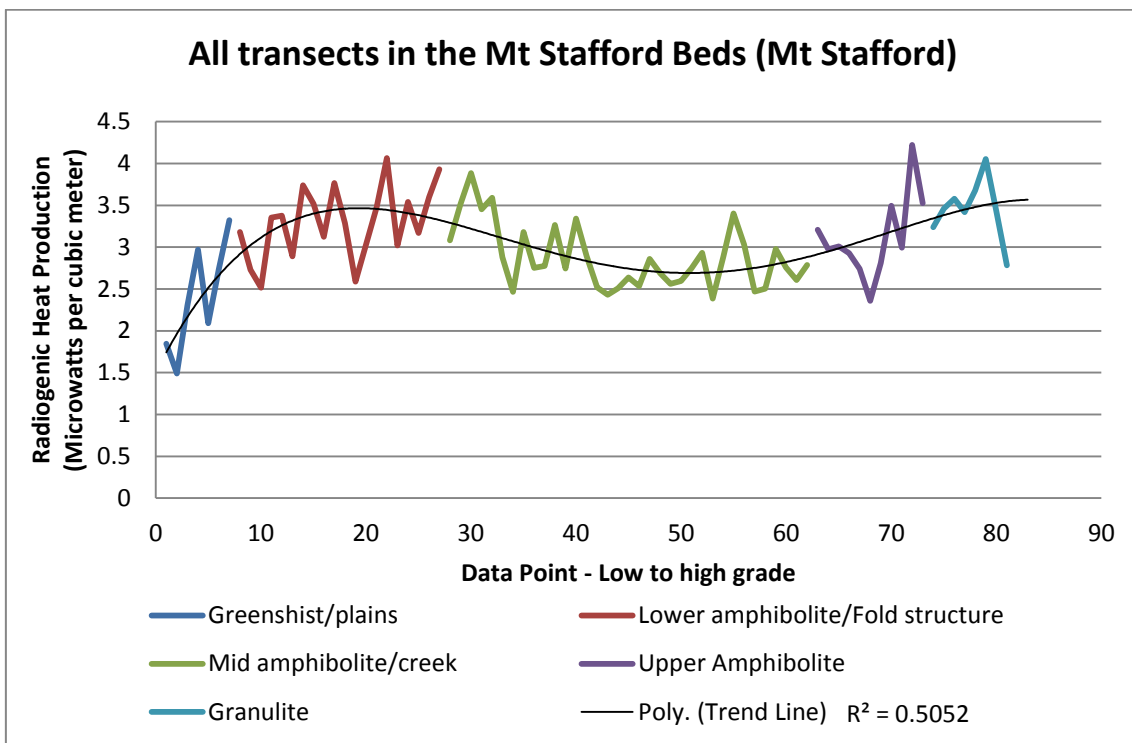
Figure 8: Heat production variation in the Mt Stafford beds, sorted by location of sample site in relation to known metamorphic grade. Each colour represents a separate transect. A trend line has been added to show the general pattern of the data.
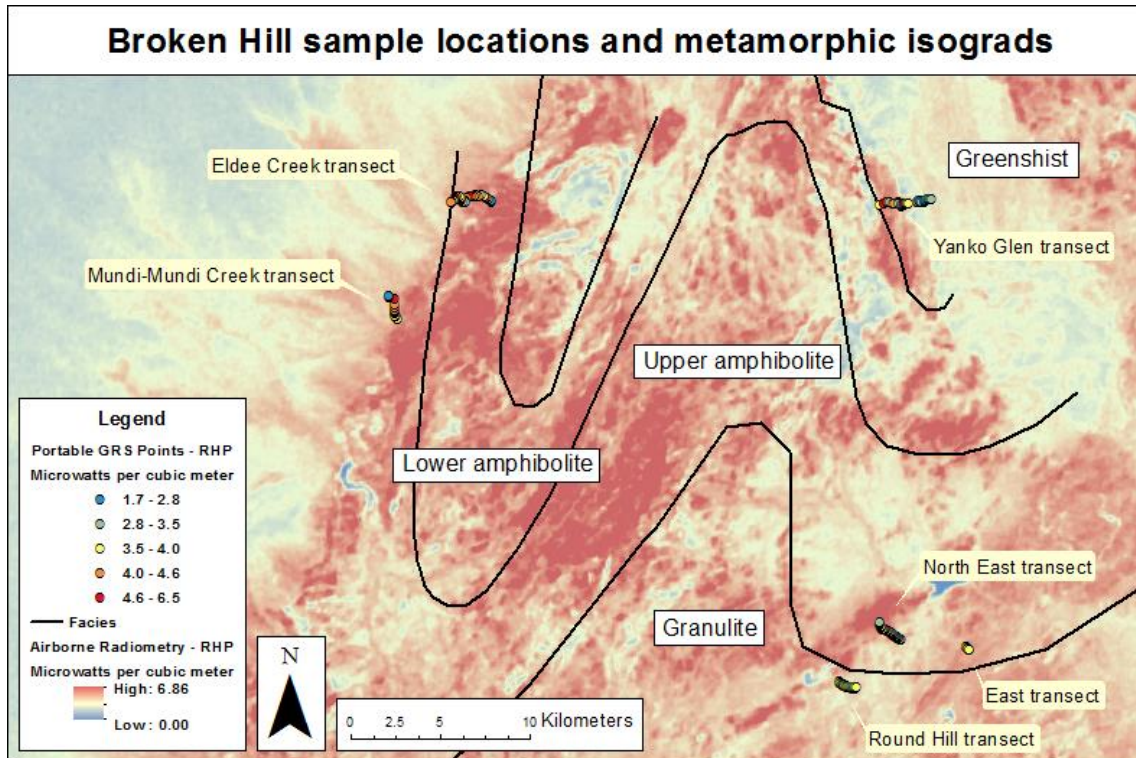
Figure 9: Locations of the sample sites at Broken Hill along with their general radiogenic heat production. RHP from airborne radiometry was calculated from separate U, Th and K layers from Geoscience Australia. The metamorphic areas are those defined by the paper by Webb and Crooks (Webb and Crooks 2005).
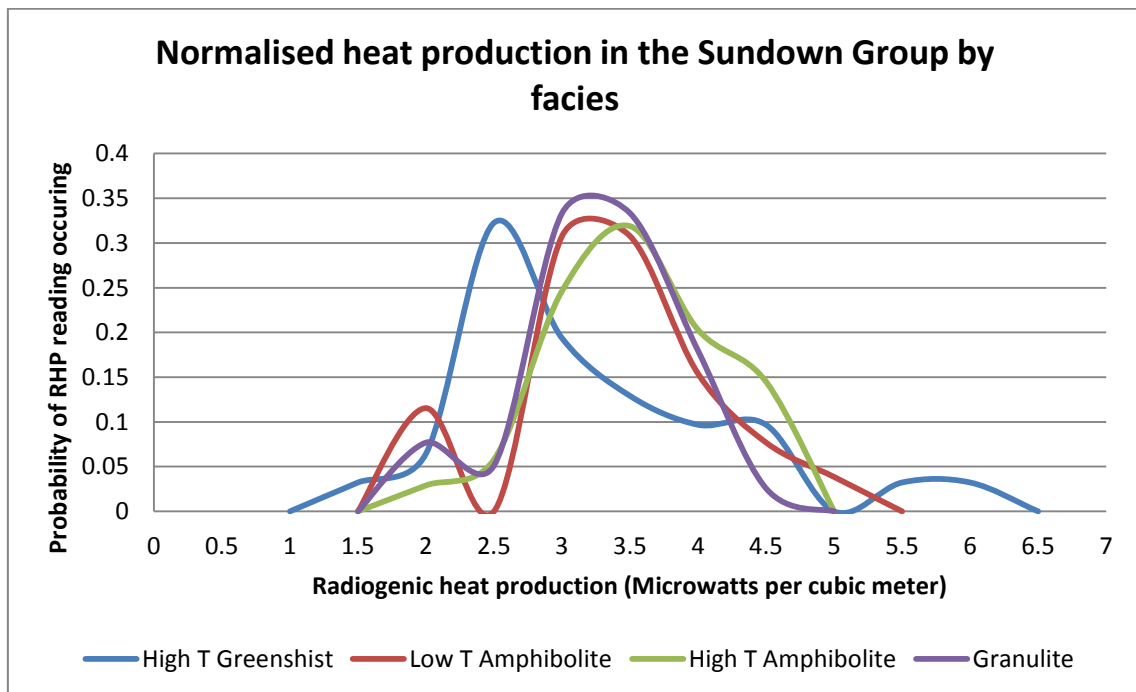
Figure 10: Normalized heat production in each of the metamorphic grades (greenschist, lower and upper amphibolite and granulite) within the Sundown group, showing the distribution of radiogenic heat production at each grade.

The plots of the calculated heat production in all three locations show similar patterns, with the granulite facies regions having higher heat production compared to lower grade equivalents (Figures 7, 10 and 13). The increase in heat production over metamorphic grade is notable at around 20%, with Mt Stafford showing an increase of around 0.5 microwatts per cubic meter and the Broken Hill and Reynolds Range showing a change of around 1 microwatt per cubic meter each.

Plots of the heat production data across metamorphic facies at each location (Figures 8, 11 and 14) show a weak pattern with a curved trend rather than a linear relation between the heat production and the metamorphic grade. The pattern is represented by an initial heat production low – greenschist – rising to a peak around the lower amphibolite facies, declining in the upper amphibolite and finally levelling out or rising again to a peak similar to or just above that of the lower amphibolite peak at the granulite facies. This pattern dominates the plots of the Mt Stafford data and is less evident in the plotted heat production values for Broken Hill. Unfortunately, the Reynolds Range set of transects only allowed for the comparison between the greenschist and granulite facies rocks, as there isn't enough data to see if this pattern exists at that location.

All three locations show an increase in thorium concentration with metamorphic grade as well as a loss of uranium with the levels of potassium remaining constant across the grades (Figure 15). While the loss in uranium across the grades decreases heat production, the significant increase in thorium serves to counter this loss, increasing overall heat production at all three field locations in their granulite domains relative to their greenschist-facies protoliths.
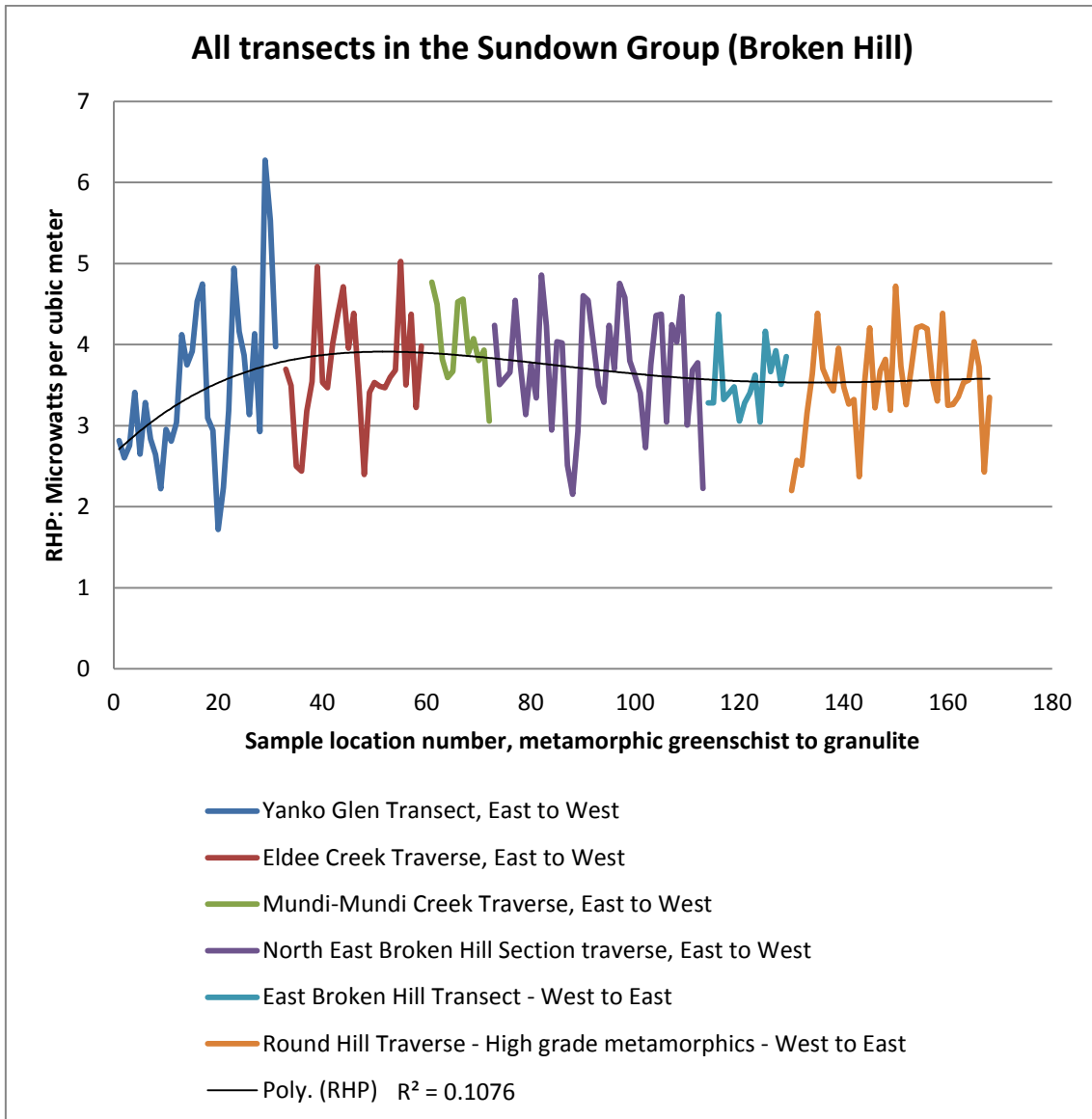
Figure 11: Heat production variation in the Sundown Group, sorted by location of sample site in relation to known metamorphic grade. Each colour represents a separate transect. A trend line has been added to show the general pattern of the data.
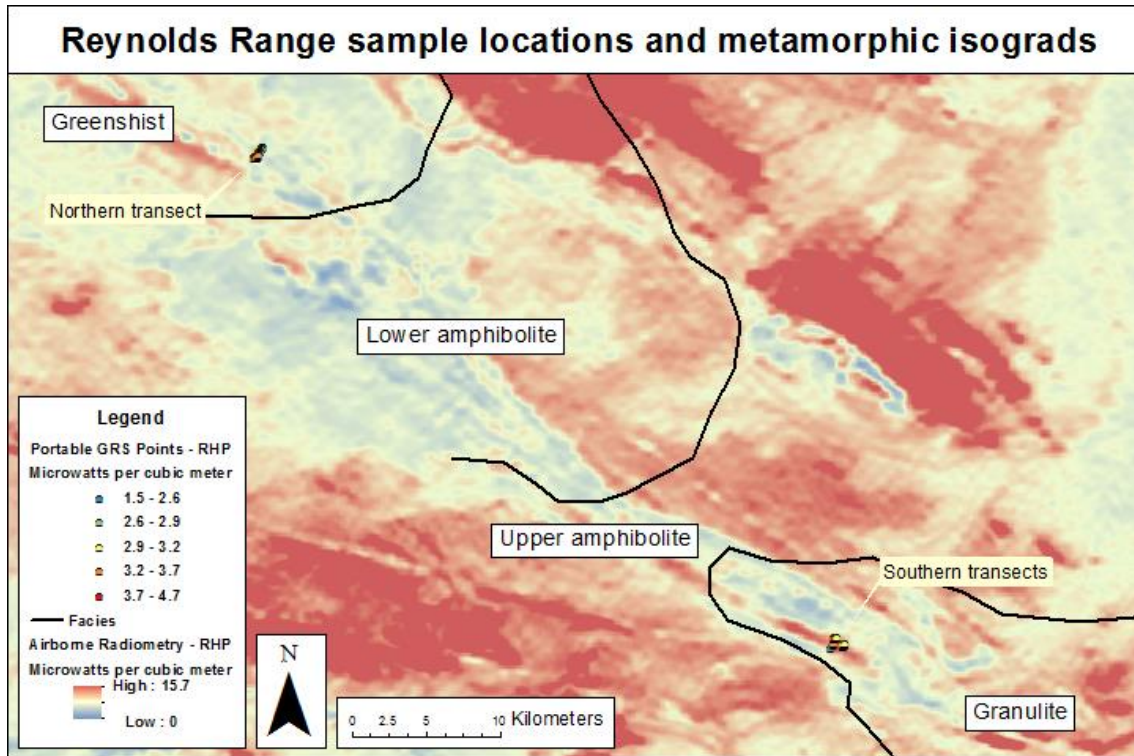
Figure 12: Locations of the sample sites within the Pine Hill Formation of the Reynolds Range along with their general radiogenic heat production (RHP). RHP from airborne radiometry was calculated from separate U, Th and K layers from Geoscience Australia. Both data sets used the method from (Rybach 1988) to calculate RHP. The metamorphic isograds are those defined in (Hand et al. 1995).
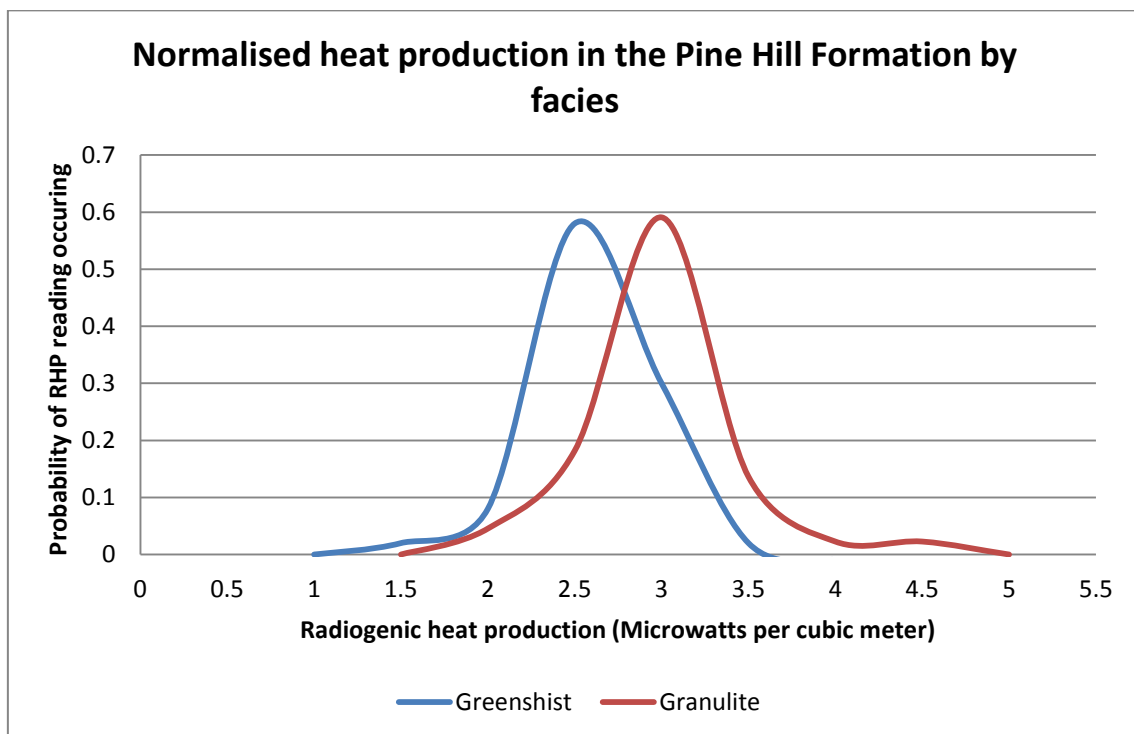
Figure 13: Normalized heat production within the Pine Hill Formation at the Reynolds Ranges.
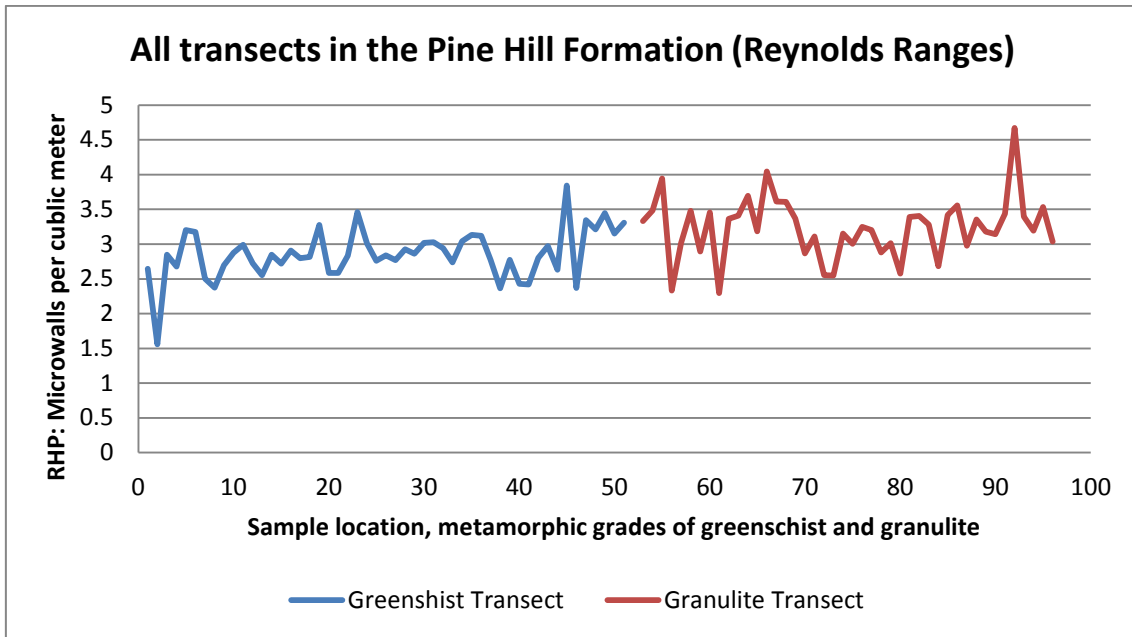
Figure 14: Heat production at the Reynolds Range, sorted by location of sample site in relation to known metamorphic grade. Each colour represents a separate transect.

4.1 Airborne radiometry comparisons:

By comparison to the GRS field measurements which targeted small-scale outcrops, the derived estimates of heat production from airborne radiometry data of the field areas show little correlation with the known metamorphic isograds. Although at one location there is notable overlap, the Mt Stafford greenschist boundary being well defined in the airborne data. This boundary would be more due to the fact that the transition into the greenschist area at Mt Stafford is also a transition into a zone with far less exposed rock which is predominately sedimentary material. This transition into sediment at the edge of the field areas can be seen in the airborne heat production data of the other two sites with the large swathes of lower heat production bounded with the fans of streams and runoff creating spreads of slightly higher heat production.

The general lack correspondence between the airborne-derived data and the data taken in situ can be explained in several ways. Firstly, although each of the selected regions

was characterised by comparatively good outcropping, at an airborne survey scale, the

land surface is dominated by recent sediment, regolith and weathered rock, all of which

are sampled indiscriminately via the airborne method. In contrast, the in situ data was

obtained from the freshest outcrops at each sampling site. Secondly the airborne data is

derived from gridded U, Th and K elemental data obtained by levelling numerous

airborne surveys against calibration flight lines. While this general approach is robust,

it is still subject to some variability created by topography and accuracy in the

calibration procedure.
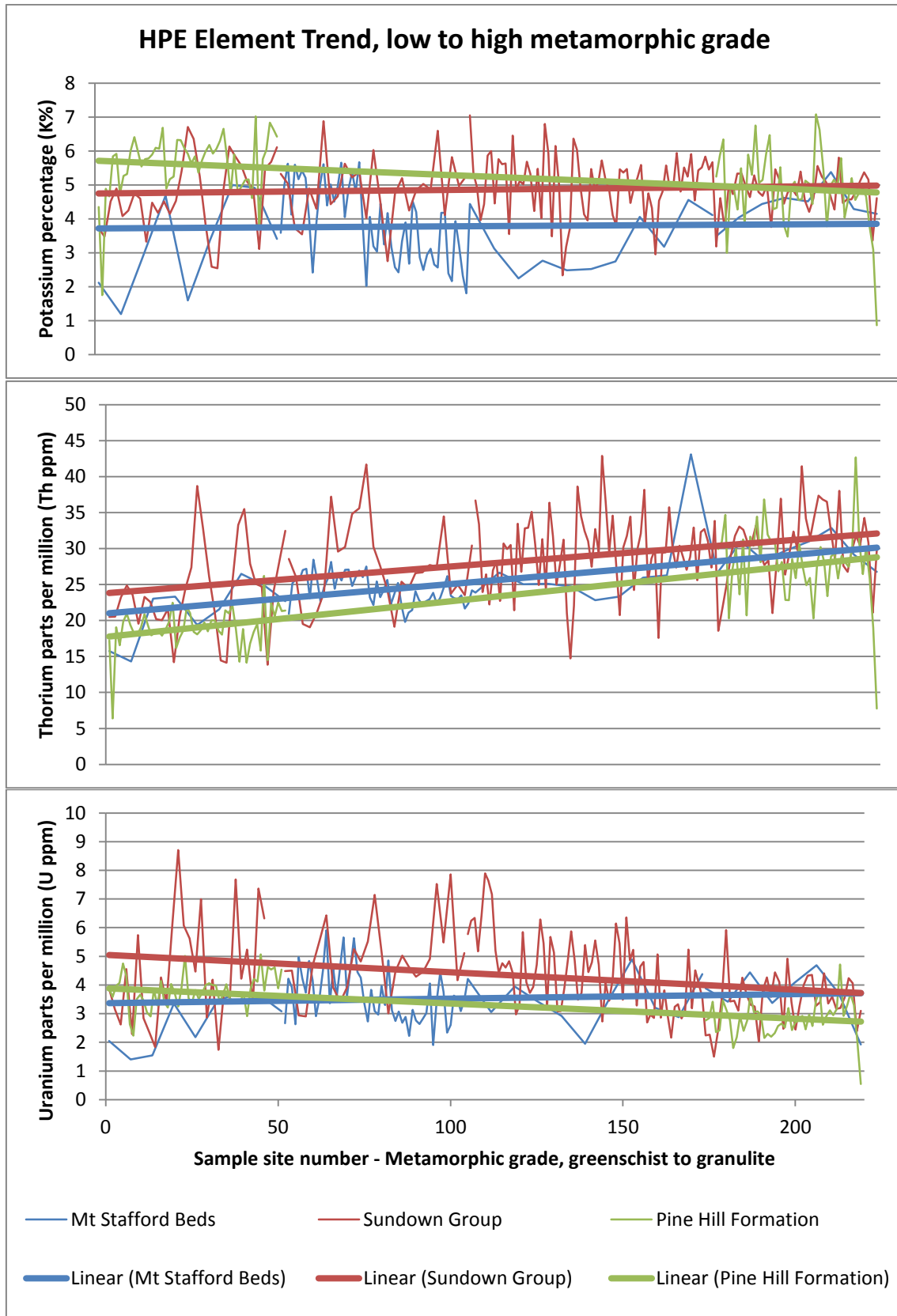
Figure 15: Potassium, thorium and uranium trends at each of the three field locations, normalised for number of samples so that each of the four metamorphic facies takes up a quarter of the plot. Trend lines have been added to show the trend of each element with increasing metamorphic grade. These plots are individually separated in Appendix 2.

4.2 Geochemical assay comparisons:

Figure 17 shows a comparison between the GRS readings and the calculated heat production from the geochemical assays from the same sample outcrops at Mt Stafford. This plot shows that although both sets of readings show similar ranges of heat production, showing the accuracy of the GRS method compared to geochemical assay, they are not very well correlated and do not follow a similar trend.

Plotting 27 of the sample locations which correlate to the Mt Stafford transects (Figure 16) shows a heat production similar to that of the GRS readings, even having a similar trend with two peaks and a central dip, but deviates, not unlike the GRS readings, from any easily readable trend. Unlike the GRS readings, the assays appear to show an overall downward trend in heat production. Additional geochemical assays could possibly show a similar trend to the GRS readings, or show that the GRS readings were biased by some unknown quantity.

The geochemical analysis of the Pine Hill Formation transects shows a similar pattern to that of the GRS data, having a higher heat production granulite peak. However, the distribution shows wider ranges of values of heat production in granulite facies rocks (Figure 18).

The overall similarity between the values determined by the GRS devices and those determined by XRF geochemical analysis are encouraging because they show that the rapid in-field assays (180 sec) of the GRS provides a reasonable estimate of the U-Th-K concentrations. However the variation between the GRS and XRD at the same location

is not surprising. The effective sample volume of the GRS approaches 0.5 m^3, whereas

the XRD determination comes from much smaller hand sample. Since the sampled

locations have sedimentary protoliths, it is likely that some variation in composition will

exist due to the differences in scale reflected by each method.
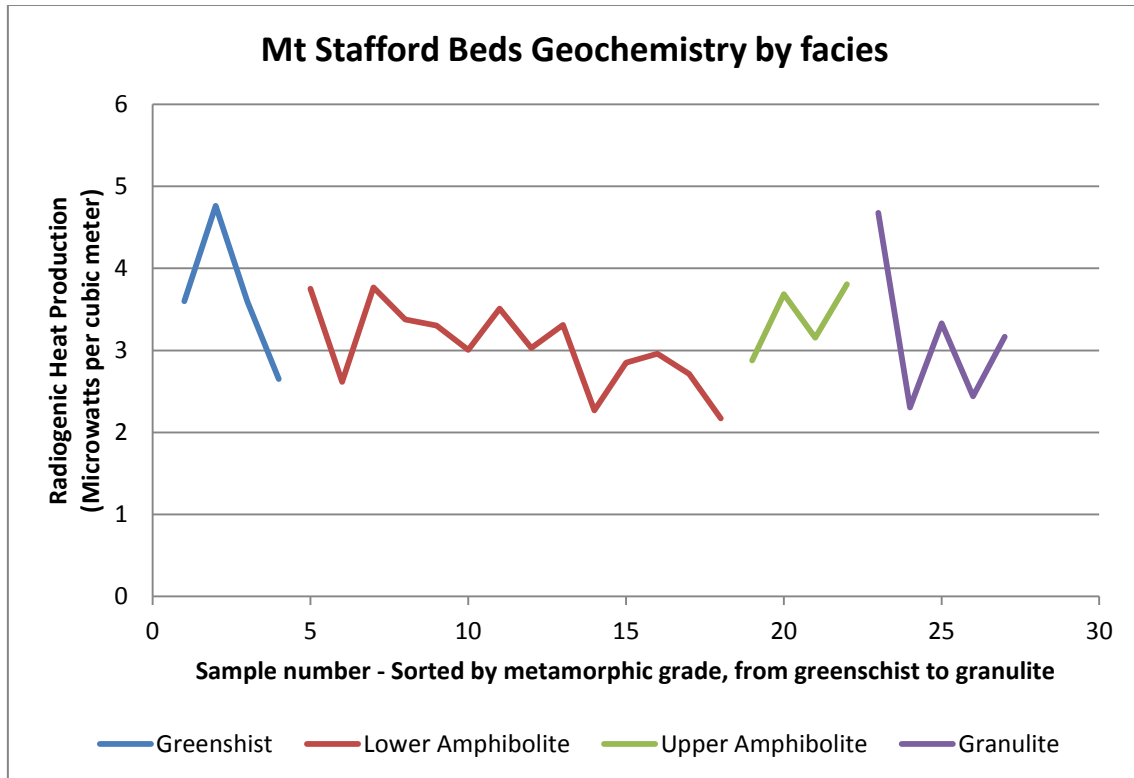
Figure 16: Plot of geochemical data at Mt Stafford, sorted by metamorphic grade and divided into metamorphic facies, with each colour representing a metamorphic facie.
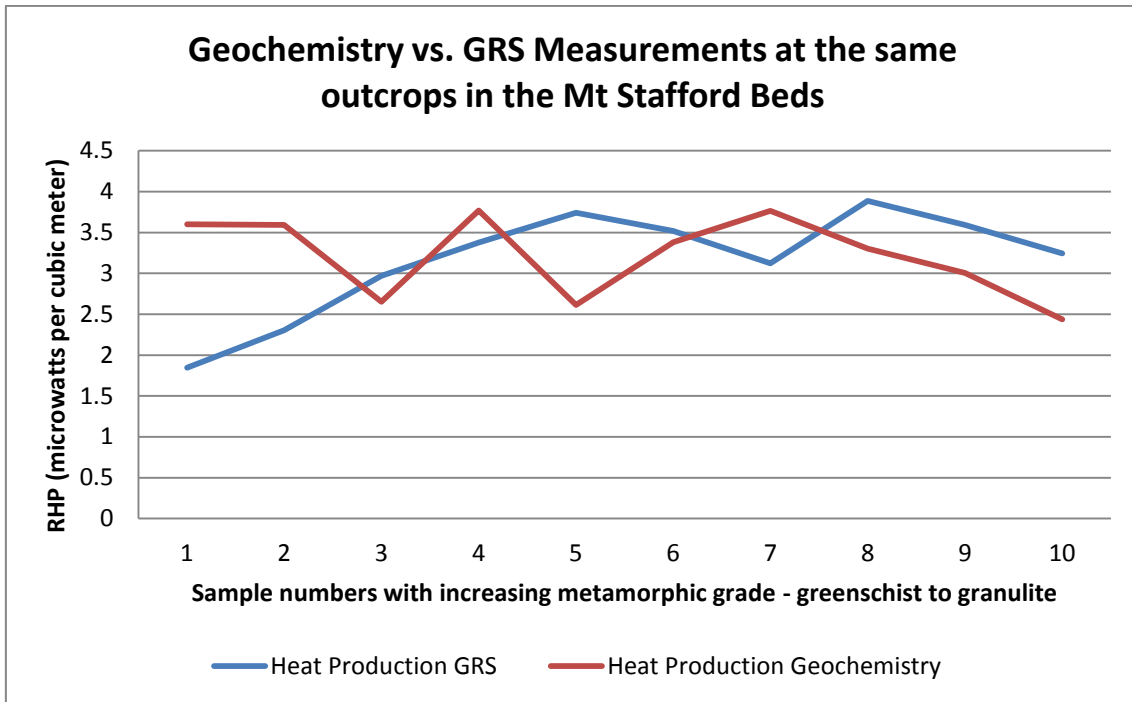
Figure 17: Comparison of XRF determination of U-Th-K data versus GRS data, using 10 data points from the same 10 outcrops, sorted by metamorphic grades, from greenschist to granulite facies rocks.
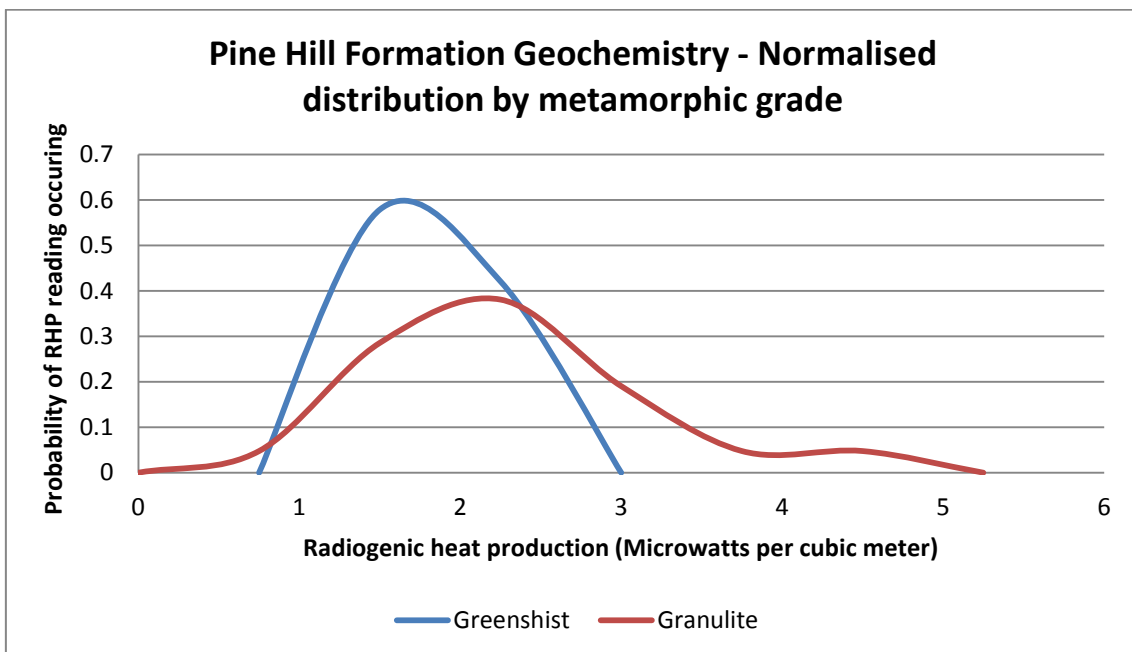
Figure 18: Normalized heat production within the Pine Hill Formation at the Reynolds Ranges from geochemical analysis.

4.3 Elemental maps

Table 2 shows analysis of elemental X-Ray maps obtained from electron microprobe compositional mapping of regions within thin sections. The proportion of each mineral was determined by counting pixels on the compositional maps of the elements that characteristically define each of the minerals in Table 2. Going from greenschist to granulite, the proportion of zircon increases both within the Mt Stafford Beds and within the Pine Hill Formation, but remains essentially the same for the Sundown Group. The proportion of monazite decreased at Mt Stafford but significantly increased in the Sundown Group and the Pine Hill. The other two HPE hosting minerals, apatite and xenotime, show higher quantities in the Sundown Group in granulite facies rocks but are lost in the Pine Hill formation.

Change in mineral quantities between greenschist and granulite grade samples

	Mt Stafford Beds	Sundown Group	Pine Hill Formation
Zircon	114% gain	Same	43% gain
Monazite	47% loss	50% gain	110% gain
Apatite	70% gain	113% gain	80% loss
Xenotime	50% loss	800% gain	25% loss
Max temp.	775-785°C	740°C	750-800°C
Max pres.	3.3-4 kbar	5 kbar	5 kbar

Table 3: The change in quantity of the HPE hosting minerals between greenschist samples and granulite samples from the element maps as a percentage (Greenschist quantity/granulite quantity, so '100% gain' indicates a doubling in quantity and 50% loss a halving). Metamorphic peak temperature and pressures for each sample site have been included for comparative purposes.

5. DISCUSSION

5.1 Analytical Considerations

There was deviation from the simple trend within the data between neighbouring sample sites of up to 7% (some at less than 20m away). The deviation in the data is directly due to observing local variations of heat producing elements within each of the rock packages. This follows the observations of Vila *et al.* (2010) in that within rock packages there are deviations from a homogenous distribution due to differences in the deposition of sedimentary beds and slightly different metamorphic and melting histories (Vilà et al. 2010). This can easily be seen in the wider distributions of some of the heat production values in the normalised distribution plots from each of the field locations, a good example can be seen in the granulite facies heat production distribution in the geochemical analysis of the Pine Hill Formation (Figure 18).

The airborne radiometry data set represents integration over a much larger area than typical ground based measurement and is biased by the inclusion of recent sedimentary and weathered material.

Each of the GRS data sets shows a definite pattern of increasing heat production with metamorphic grade. The similarities in heat production across all three sites would indicate that this pattern is not isolated to only one locality, but rather more widespread. This differs from the general understanding that granulite facies rocks are depleted in heat producing elements (Vigneresse et al. 1989, McLaren et al. 2003, Gazzaz and Hashad 1991, Ashwal et al. 1987). To understand why this change has occurred the

HPE bearing minerals monazite and zircon are examined, along with the patterns of heat production determined by data collected in the field.

At all of the study locations the prograde metamorphic path rises through 740 degrees Celsius, close to the point at which we start to lose HPE bearing minerals. This is the boundary between the upper amphibolite and lower granulite facies, where first melting begins to take place, with increasing temperature from this boundary dry melting without fluid also occurs (Collins 2000, Collins and Vernon 1991, Page and Laing 1992, Vry et al. 1996, Williams et al. 1996). At these temperatures and in the presence of melt monazite crystals begin to break down, dissolving into the melt. At around 740°C, zircons only start to melt and crystals may remain up until around 900°C, again depending on the pressure of the system and the composition of the melt (Yakymchuk and Brown 2014, Kelsey et al. 2008). As the results show a rise in HPEs at higher temperatures in the granulite facies rocks, it can be inferred that most of the monazites or zircons remain within the residual post-partial melt rock, increasing its relative radiogenic heat production. Geochemical analysis of the samples from the Pine Hill Formation show an increase in zirconium, indicating zircons remaining after partial melt removal. The Pine Hill Formation also shows an increase in both zircon and monazite crystals in the element maps.

Differing pressure/temperature (P-T) conditions at each of the field sites should effect the percentage of monazite and zircon remaining in the residual rock. Notably, the Sundown Group reached higher temperatures in the granulite facies zones than the other two field sites, up to 800°C (Page and Laing 1992). From Kelsey *et al.* (2008), it can be

seen that at a concentration of 250ppm zircon in a metapelitic rock, 25% of the zircons will be dissolved into the melt phase. At lower concentrations, around 50ppm, all of the zircons will be dissolved (Kelsey et al. 2008). To test the theory of a complete melting of the zircons at any of the field sites, zircon dating can be used to see whether all of the zircons have the same date (all melted at one point) or whether only partial melts occurred (multiple dates found). The Sundown Group at Broken Hill was tested by Page *et al.* (2005) and was found to be full of detrital zircons dated around 1780-1790 Ma, indicating that none of the zircons within the group were dissolved even partially into the melt.

Similarly, the lower pressures measured at Mt Stafford, around 3.3 kbar rather than the 5 kbar at the other field sites (Collins and Vernon 1991, Page and Laing 1992, Collins 2000), could have contributed to the trend pattern visible in the Mt Stafford transect data (Figure 8), a pattern which is weaker but possibly in the Broken Hill transect.

The pressure/temperature stability of monazite and zircon crystals is important for gauging when the crystals break down and become part of the melt, but the zircon and monazite crystals themselves may be transported by the melt. The crystals may remain a part of the transport of the HPEs without becoming part of the melt phase (Yakymchuk and Brown 2014). Transport of any percentage of the HPEs regardless of whether they are still in a crystalline form or free within the melt will affect the distribution of heat production within the rocks and so the results of this study. Transport of HPE via whole crystals could be tested by comparing the dates of zircons (U/Th) which should be older than the dates of the melt products (K/Ar) (Dunkley et al. 2008). Loss of melt in a

system leads to volume loss, and loss of volume increases the concentrations of the minerals which didn't dissolve into the melt as they form a residual rock. Thus, even if the HPEs are transported in hosting minerals within the melt and deposited in a new rock, if the melt continues to move after the deposition of the intact HPE hosting minerals, the same enrichment process will take place.

Elementary breakdown of the GRS data yields several patterns that could be used to infer the order of melting (Figure 15). Most notable is the increase in thorium while a decrease in potassium and uranium occurs. While uranium has the largest effect on heat production, at over 3 and a half times greater than thorium and far greater than potassium, at 2700 times (Vilà et al. 2010), the 20 parts per million increase in thorium over metamorphic grade acts to counter the heat production lost with the small amount of uranium lost. The fact that thorium alone is responsible for the increase in heat production could be linked to the mineralogy of the field areas studied. A study of the location of thorium within the HPE bearing minerals as metamorphic grade increases should help with understanding this trend.

The element mapping shows that the quantities of each of the HPE bearing minerals in each of the field areas changes as with metamorphic grade (Table 2). Depending on the original concentration, different minerals may survive longer under increasing P-T conditions. Similarly, if a system is open and melt can escape continuously, it is harder to dissolve minerals with high melting points due to the remaining melt already being saturated and existing in smaller quantities (Yakymchuk and Brown 2014, Kelsey et al. 2008). All of the field sites show a relative gain in thorium (Figure 15) and HPE bearing

minerals over metamorphic grade (Table 2), so the melt must have been extracted

before the threshold at which these minerals dissolve easily (Yakymchuk and Brown

2014). Unfortunately, due to the resolution of the element maps at 20x20mm each, it is

impossible to directly identify the location of HPE bearing elements directly within the

minerals as the minerals in which they reside are too small to be resolved as anything

more than a few pixels wide. An indication that the thorium concentration in the

minerals may vary can be seen in the geochemistry data from the Pine Hill Formation.

Notably, as monazite is a Ce-La phosphate, with decreasing concentrations of these

minerals as we go from greenschist to granulite that we can see in the data (see

Appendix 4), we would expect there to be a corresponding decrease in thorium as it is

also hosted in the monazite. We instead find an increase in thorium, which leads us to

the conclusion that the monazites present hosting the thorium in the granulite zone are

enriched in thorium compared to those in the greenschist zone.

Along with the movements of elements via partial melting, it should be noted that there

are other metamorphic processes besides partial melting by which HPE concentrations

can be changed. Metamorphic rocks devolitise with progressive metamorphism (Ague

1991). Hence metamorphic fluid could remobilize soluble HPEs, particularly uranium,

via dehydration reactions and fluid flow (Vilà et al. 2010). Of the three field locations,

Broken Hill, due to large-scale alteration, would reflect this kind of change in the data

(Page and Laing 1992). In the uranium data from Broken Hill, the data shows greater

variability, deviating notably from a general trend (Figure 15 and separated out in

Appendix 2). This deviation could possibly be due to differing levels of fluid alteration

having an effect on the concentration of uranium between each of the sample points and

transects, a pattern which, while present, isn't as strong at either of the two other field areas.

Numerical modelling of orogenic processes relies on understanding heat production distribution to show where strengthening and weakening is occurring in the lithosphere (Hasterok and Chapman 2011, Sandiford and McLaren 2002). Concentration of HPEs at shallow crustal depth cools and so strengthens the lower crust, while concentrations of HPEs in the lower crust can lead to elevated thermal regimes, easing deformation and so weakening the lower crust. Due to re-working of the crust, overlapping metamorphic events could lead to a dispersed HPE concentration and hence stronger overall crust due to steeper geotherms. This is known as tectonic lock and is one of the major processes in the creation of stable cratonic style crust (Sandiford et al. 2001, Sandiford and McLaren 2002, Perry et al. 2006).

Increasing thorium (Figure 15) and HPE bearing mineral quantities (Table 2) show that the concentration of HPEs in the metamorphic systems at all three field sites is high enough to enrich HPEs in these rocks. The study areas are then on the other side of a global threshold with a higher than global average heat production (Sandiford et al. 2001), allowing them to avoid tectonic lock as has been seen in other sites around the world. The self-enriching HPE systems of central Australia as shown in this paper are hence the probable cause for some of the largest intracratonic orogens on Earth, the Peterman and Alice Springs orogenies (Kennett and Iaffaldano 2013, Klootwijk 2013, Belton et al. 2004, Roberts and Houseman 2001).

5.2 Further study

Due to the nature of the findings – the contradiction of the common understanding of the lower heat production in granulite facies and the trend dominating heat production distribution – additional study of other sites with larger data sets along with verification data from the sites used in this paper will result in a better understanding and help to reduce any unknowns that may be affecting the results.

The set of traverses at Mt Stafford had gaps due to lack of time in the field (note Mt Stafford map Figure 6). Due to the shorter distance across metamorphic grade, further study should allow for the creation of a single 10km traverse at Mt Stafford, encompassing the entirety of the metamorphic grade from greenschist to granulite facies.

Similarly, the Pine Hill Formation in the Reynolds Range data lacks both the upper and lower amphibolite heat production data. Additional traverses to fill in the gaps may yield more information about the trend pattern found in the heat production at the other two sites.

To further study the relationship between the airborne, portable GRS and geochemical data, a site that has extensive outcropping would need to be studied by all three methods in parallel. Due to the granularity of the airborne data and the lack of geochemical samples taken in the field compared to the number of portable GRS measurements, it is difficult to draw any definite conclusions about the differences between the methods in this paper.

6. CONCLUSIONS

The results of this study indicate that there is a definite correlation between the increase of metamorphic grade and an increase in heat production at Mt Stafford, Broken Hill and the Reynolds Ranges, due to the concentration of heat producing elements being high enough to further enrich themselves during partial melting. This was driven mostly by the element thorium remaining due to its presence in residual minerals after possible continuous open system partial melting occurred.

Field testing the portable gamma ray spectrometry units showed that they are a tool which provides a good bulk average heat production, solving the aforementioned issues with using airborne radiometry, along with removing the inherent heterogeneity of materials when performing a geochemical assay. The GRS units perform comparatively accurately to geochemical analysis over a much smaller time frame, allowing for large sample sets to be collected over the same amount of time.

7. ACKNOWLEDGMENTS

REFERENCES

AGUE J. J. 1991 Evidence for major mass transfer and volume strain during regional metamorphism of pelites, *Geology,* vol. 19, pp. 855-858.

ANDREOLI M. A. G., HART R. J., ASHWAL L. D. & COETZEE H. 2006 Correlations between U, Th Content and Metamorphic Grade in the Western Namaqualand Belt, South Africa, with Implications for Radioactive Heating of the Crust, *Journal of Petrology,* vol. 47, no. 6, pp. 1095-1118.

ASHWAL L. D., MORGAN P., KELLEY S. A. & PERCIVAL J. A. 1987 Heat production in an Archean crustal profile and implications for heat flow and mobilization of heat-producing elements, *Earth and Planetary Science Letters,* vol. 85, no. 4, pp. 439-450.

BEA F. 2012 The sources of energy for crustal melting in geochemistry of heat-producing elements, *Lithos,* vol. 153, pp. 278-291.

BELTON D. X., BROWN R. W., KOHN B. P., FINK D. & FARLEY K. A. 2004 Quantitative resolution of the debate over antiquity of the central Australian landscape: implications for the tectonic and geomorphic stability of cratonic interiors, *Earth and Planetary Science Letters,* vol. 219, no. 1-2, pp. 21-34.

BRADY R. J., DUCEA M. N., KIDDER S. B. & SALEEBY J. B. 2006 The distribution of radiogenic heat production as a function of depth in the Sierra Nevada Batholith, California, *Lithos,* vol. 86, no. 3–4, pp. 229-244.

BUICK I. S., CARTWRIGHT I. & HARLEY S. L. 1998 The retrograde P–T–t path for low-pressure granulites from the Reynolds Range, central Australia: petrological constraints and implications for low-P/high-T metamorphism, *Journal of Metamorphic Geology,* vol. 16, no. 4, pp. 511-529.

CHRISTENSEN N. I. & MOONEY W. D. 1995 Seismic velocity structure and composition of the continental crust: a global view, *Journal of Geophysical Research,* vol. 100, pp. 9761-9788.

COLLINS W. J. 2000 Granite magma segregation and transfer during compressional deformation in the deep crust? Proterozoic Arunta Inlier, Central Australia Conference Excursion Guide*.* 15th Australian Geological Congress.

COLLINS W. J. & SHAW R. D. 1995 Geochronological constraints on orogenic events in the Arunta Inlier, a review, *Precambrian Research*, no. 71, pp. 315-346.

COLLINS W. J. & VERNON R. H. 1991 Orogeny associated with anticlockwise P---T---t paths: evidence from low-P high-T meta-morphic terranes in the Arunta Inlier, central Australia, *Geology*, no. 19, pp. 835-838.

DIRKS P. H. G. M. 1990 Intertidal and subtidal sedimentation during a mid-Proterozoic marine transgression, reynolds range group, Arunta block, central Australia, *Australian Journal of Earth Sciences,* vol. 37, no. 4, pp. 409-422.

DUNKLEY D. J., SUZUKI K., HOKADA T. & KUSIAK M. A. 2008 Contrasting ages between isotropic chronometers in granulites: monazite dating and metamorphism in the Higo complex, Japan, *Gondwana Research*, no. 14, pp. 624-643.

FORBES C. J., BETTS P. G., GILES D. & WEINBERG R. 2008 Reinterpretation of the tectonic context of high-temperature metamorphism in the Broken Hill Block, NSW, and implications on the Palaeo- to Meso-Proterozoic evolution, *Precambrian Research,* vol. 166, pp. 338-349.

FORBES C. J., BETTS P. G., WEINBERG R. & BUICK I. S. 2005 A structural metamorphic study of the Broken Hill Block, NSW, Australia., *Journal of Metamorphic Geology*, no. 23, pp. 745-770.

FOUNTAIN D. M. & RUDNICK R. L. 1995 Nature and composition of the continental crust: A lower crustal perspective, *Reviews of Geophysics,* vol. 33, no. 3, pp. 267-309.

GAZZAZ M. A. & HASHAD A. H. 1991 Radiogenic heat production and heat flow in the northern Arabian Shield, *Journal of African Earth Sciences (and the Middle East),* vol. 13, no. 3–4, pp. 323-332.

GRAESSNER T. & SCHENK V. 2000 An Exposed Hercynian Deep Crustal Section in the Sila Massif of Northern Calabria: Mineral Chemisty, Petrology and a P-T Path of Granulite-facies Metapelitic Migmatites and Metabasites, *Journal of Petrology,* vol. 42, no. 5, pp. 931-961.

GREENFIELD J. E., CLARKE G. L., BLAND M. & CLARK D. J. 1996 In-situ migmatite and hybrid diatexite at Mt Stafford, central Australia, *Journal of Metamorphic Geology,* vol. 14, pp. 413-426.

GREENFIELD J. E., CLARKE G. L. & WHITE R. W. 1998 A sequence of partial melting reactions at Mt Stafford, central Australia, *Journal of Metamorphic Geology,* vol. 16, pp. 363-378.

HAND M. & BUICK I. S. 2001 Tectonic evolution of the Reynolds-Anmatjira Ranges: a case study in terrain reworking from the Arunta Inlier, central Australia, *Geological Society, London, Special Publication*, no. 184, pp. 237-260.

HAND M., FANNING C. M. & SANDIFORD M. 1995 Low-P High metamorphism and the role of high-heat producing granites in the northern Arunta Inlier, *Australian Geological Society, Abstracts*, no. 40, pp. 60-61.

HASTEROK D. & CHAPMAN D. S. 2011 Heat production and geotherms for the continental lithosphere, *Earth and Planetary Science Letters,* vol. 307, pp. 59-70.

HOBBS B. E., ARCHIBALD N. J., ETHERIDGE M. A. & WALL V. J. 1984 Tectonic history of the Broken Hill Block, Australia. Schweizerbartische, Stuttgart.

KELSEY D. E., CLARK C. & HAND M. 2008 Thermobarometric modelling of zircon and monazite growth in melt-bearing systems: examples using model metapelitic and metapsammitic granulites, *Journal of Metamorphic Geology,* vol. 26, pp. 199-212.

KELSEY D. E. & POWELL R. 2010 Progress in linking accessory mineral growth and breakdown to major mineral evolution in metamorphic rocks: a thermodynamic approach in the NA2O-CaO-K2O-FeO-MgO-Al2O3-SiO2-H2O-TiO2-ZrO2 system, *Journal of Metamorphic Geology,* vol. 19, no. 1, pp. 151-166.

KENNETT B. L. N. & IAFFALDANO G. 2013 Role of lithosphere in intra-continental deformation: Central Australia, *Gondwana Research,* vol. 24, no. 3-4, pp. 958-968.

KLOOTWIJK C. 2013 Middle–Late Paleozoic Australia–Asia convergence and tectonic extrusion of Australia, *Gondwana Research,* vol. 24, no. 1, pp. 5-54.

KUMAR S., P., MENON R. & REDDY G. K. 2007 The role of radiogenic heat production in the thermal evolution of a Proterozoic granulite-facies orogenic belt:

Eastern Ghats, Indian Shield, *Earth and Planetary Science Letters,* vol. 254, pp. 39-54.

LUDWIG K. 2014 Isoplot Excel addon. 4.1 ed.: Berkeley Geochronology Centre (BGC).

MARESCHAL J.-C. & JAUPART C. 2013 Radiogenic heat production, themal regime and evolution of continental crust, *Tectonophysics.*

MAWBY J., HAND M. & FODEN J. 1999 Sm/Nd evidence for high-grade Ordovician metamorphism in the Arunta Block, central Australia, *Journal of Metamorphic Geology*, no. 17, pp. 653-668.

MCLAREN S., SANDIFORD M., HAND M., NEUMANN N., WYBORN L. & BASTRAKOVA I. 2003 The hot southern continent: heat flow and heat production in Australian Proterozoic Terranes. Geological Society of Australia Special Publication. pp. 151-161.

MINTY B. R. S., FRANKLIN R., MILLIGAN P. R., RICHARDSON L. M. & WILFORD J. 2010 Radiometric Map of Australia. 2nd ed. Canberra: Geoscience Australia.

PAGE R. W. & LAING W. P. 1992 Felsic metavolcanic rocks related to the Broken Hill Pb–Zn–Ag orebody, Australia: geology, depositional age, and timing of highgrade metamorphism, *Economic Geology*, no. 87, pp. 2138-2168.

PAGE R. W., STEVENS B. P. J. & GIBSON G. M. 2005 Geochronology of the sequence hosting the Broken Hill Pb–Zn–Ag orebody, Australia, *Economic Geology Bulletin, Society of Economic Geologists*, no. 100, pp. 633-661.

PAGE R. W., STEVENS B. P. J., GIBSON G. M. & CONOR C. H. H. 2000 Geochronology of Willyama Supergroup rocks between Olary and Broken Hill, and comparison to Northern Australia, *Australian Geological Survey Organisation Record*, no. 2000/10, pp. 72-75.

PERRY H. K. C., JAUPART C., MARESCHAL J.-C. & BIENFAIT G. 2006 Crustal Heat Production in the Superior Province, Canadian Shield, and in North America inferred from heat flow data, *Journal of Geophysical Research,* vol. 111, pp. 1-20.

RAY L., ROY S. & SRINIVASAN R. 2008 High radiogenic heat production in the Kerala Khondalite Block, Southern Granulite Province, India, *International Journal of Earth Science,* vol. 97, pp. 257-267.

ROBERTS E. A. & HOUSEMAN G. A. 2001 Geodynamics of central Australia during the intraplate Alice Springs Orogeny: thin viscous sheet models, *Geological Society of London Special Publication,* vol. 184, pp. 139-164.

RUBATTO D., HERMANN J. & BUICK I. S. 2006 Temperature and Bulk Composition Control on the Growth of Monazite and Zircon During Low-pressure Anatexis (Mount Stafford, Central Australia), *Journal of Petrology,* vol. 47, no. 10, pp. 1973-1996.

RYBACH L. 1988 Determination of heat production rate*,* Kluwer Academic Press.

SANDIFORD M., HAND M. & MCLAREN S. 2001 Tectonic feedback, intraplate orogeny and the geochemical structure of the crust: a central Australian perspective, *Continental Reactivation and Reworking,* vol. 184, pp. 195-218.

SANDIFORD M. & MCLAREN S. 2002 Tectonic feedback and the ordering of heat producing elements within the continental lithosphere, *Earth and Planetary Science Letters,* vol. 204, no. 1–2, pp. 133-150.

SANDIFORD M., MCLAREN S. & NEUMANN N. 2002 Long-term thermal consequences of the redistribution of heat producing elements associated with large-scale granitic complexes, *Metamorphic Geology,* vol. 20, no. 1, pp. 87-98.

SPEAR F. S. 1993 Metamorphic Phase Equilibria & Pressure-Temperature-Time Paths. Bookcrafters, Inc., Michigan, USA.

STEVENS B. P. J., BARNES R. G., BROWN R. E., STROUD W. J. & WILLIS I. L. 1988 The Willyama Supergroup in the Broken Hill and Euriowie Blocks, New South Wales, *Precambrian Research*, no. 40-41, pp. 297-327.

STEWART A. J. 1981 Reynolds Range Region, Northern Territory, 1:100000 Geological Map Commentary. Canberra, A.C.T.: Bureau of Mineral Resources, Geology and Geophysics.

TAYLOR S. R. & MCLENNAN S. M. 1995 The Geochemical Evolution of the Continental Crust, *Reviews of Geophysics*, no. 33, pp. 241-265.

VIGNERESSE J. L., BARBEY P. & CUNEY M. 1996 Rheological transitions during partial melting and crystalization with application to felsic magma segregation and transfer, *Journal of Petrology,* vol. 37, pp. 1579-1600.

VIGNERESSE J. L., CUNEY M., JOLIVET J. & BIENFAIT G. 1989 Selective heat-producing element enrichment in a crustal segment of the mid-European Variscan chain, *Tectonophysics,* vol. 159, no. 1–2, pp. 47-60.

VILÀ M., FERNÁNDEZ M. & JIMÉNEZ-MUNT I. 2010 Radiogenic heat production variability of some common lithological groups and its significance to lithospheric thermal modeling, *Tectonophysics,* vol. 490, no. 152-164.

VRY J., COMPSON W. & CARTWRIGHT I. 1996 SHRIMP II dating of zircons and monazites: reassessing the timing of high-grade metamorphism and fluid flow in the Reynolds Range, northern Arunta Block, Australia., *Journal of Metamorphic Geology*, no. 14, pp. 335-350.

WARREN R. G. 1983 Metamorphic and tectonic evolution of granulites, Arunta Block, central Australia, *Nature,* vol. 305, pp. 300-303.

WEBB G. & CROOKS A. 2005 Metamorphic investigation of the Palaeoproterozoic metasediments of the Willyama Inliers, southern Curnamona Province — a new isograd map, *MESA Journal,* vol. 37, pp. 53-57.

WHITE R. W., POWELL R. & CLARKE G. L. 2003 Prograde Metamorphic Assemblage Evolution during Partial Melting of Metasedimentary Rocks at Low Pressures: Migmatites from Mt Stafford, Central Australia, *Journal of Petrology,* vol. 44, no. 11, pp. 1937-1960.

WILLIAMS I. S., BUICK I. S. & CARTWRIGHT I. 1996 An extended episode of early Mesoproterozoic metamorphic fluid flow in the Reynolds Range, central Australia, *Journal of Metamorphic Geology*, no. 14, pp. 29-47.

YAKYMCHUK C. & BROWN M. 2014 Behavior of zircon and monazite during crustal melting, *Journal of the Geological Society, London.*

APPENDIX 1: GRS FIELD SAMPLING METHODS

For sampling outcrops in the field, I used the Radiation Solutions (RS) RS 230 BGO SuperSpec devices, which are handheld portable gamma ray spectrometers. I used four of the devices in parallel, primarily to reduce the variation in element concentration that may occur across a few meters of outcrop. The multiple devices also allowed for reduction of error and elimination of outliers via comparison between the devices. The four devices were compared to one another over each week of field sampling to see whether they started to drift apart. To eliminate possible drift in all four devices over the week, two readings were taken of the same good quality outcrop by all four devices, once at the start and once at the end of the week.

Pre-use:
Before planning field work, calibrate the devices to a known standard – in this case the calibration pads at the DIMITRE yard at Thebarton in Adelaide. Before the first sampling trip, I made sure that the devices had been calibrated recently, in that case only a few months prior. For all subsequent trips, I calibrated the devices myself using the manufacturer's instructions and took a set of readings for comparison before leaving for the field.

Manuals and farther technical information of the RS 230 devices can be found by contacting Radiation Solutions and on this information page:
http://www.radiationsolutions.ca/index.php?id=78

In the field:
Make sure that all of the devices that you are going to use in the field have fresh battery packs and that you have replacements carried with you. For these devices, each of the battery packs should last for 8 hours, depending on the quality of AA batteries used.

Taking samples:
Make sure that the devices are on and stabilized to the background. If they are off, or it is the first sample site of the day, wait to make sure that they are turned on and left for at least 10 minutes after initial stabilization in order to stabilize them properly. If they have low batteries while in the field, turn them off, wait 15 seconds, replace the battery packs and leave to stabilize for another 10 minutes.

Place the devices on the outcrop with the flat front plates of the devices acting as their bases as flush as you can against the rock. If you can't find great outcrop, try to place the devices to cover all the best exposures within 3m of each other, keeping in mind that the active detection area of the devices is around the first half cubic meter around the head of the device. Any outcrop you place the devices on should have as much of this half cubic meter as possible filled with the rock to be sampled, with each device having a similar amount of rock within that half cubic meter.

Begin the Assay process on all the devices. For this study, the devices were set up to run for 180 seconds, 3 minutes of detection time. This time was chosen due to Radiation Solutions' recommendation that the devices could return very accurate readings over

this time. It also allowed more samples to be taken in the day than a longer assay time may have.

When the devices have completed their assays, I recorded their readings of the concentration of potassium, uranium and thorium along with the displayed dose of radiation and the assay number, for future reference and error checking. I also recorded a GPS location for each sample point and noted this down for classification of the sample location metamorphic grade with regards to other literature on the field site. The last datum recorded for each site is a record of outcrop quality, ranging from 1 indicating mostly alluvium and difficult to track outcrop with a large amount of cobbles or other rocks on the surface as float to 10, indicating the outcrop is flat and wide, with a well exposed surface devoid of dirt, float or plant life.

An example of the two ends of the quality scale can be found with the barely exposed almost metamorphosed sediment generally having a quality as low as 1, while the large areas of granite at the other end of the scale gained several outcrop ratings of 10. The outcrop quality was noted so that low quality sample sites could then be found and removed if they are statistical outliers due to their larger error bands. The readings and associated information taken down at each sample location was written down on a clipboard on pre-printed form paper with pen. The total readings for the Mt Stafford field trip totalled 11 and a half single sided A4 pages.

The devices are then returned to their base state, a normal scanning mode and carried to the next sample location, where the process is repeated. For the sampling trips, the devices were left on for as long as possible to ensure that they were stabilized across all of the samples taken on that day.

After returning from fieldwork:
After the first round of fieldwork at Mt Stafford, the devices were taken back to the calibration pads in Thebarton and used to test the pads known concentrations. This gave an idea of the difference between the device's readings and the actual quantities and allowed for the calculation of offset multipliers to correct the data taken in the field. The corrections were calculated by a method as follows:

1. With each of the four devices, I ran 180 second assays on each of the three pads (potassium, uranium and thorium) twice.
2. I averaged these values for each device on each pad (my values do not differ between the two assays by more than 3%)
3. I compared these values of concentration to those known for the pads and found what number I needed to multiply the taken value by to gain the known value. This multiplier was then applied to all the readings taken in the field to correct them.
4. The method of correction could be used as I saw no major difference in the readings taken on the same outcrop between the start and the end of the week of fieldwork. For subsequent trips, the number of readings to find a baseline was increased, up to 12 readings, to improve the average found and so the quality of the multiplier used.

Confirming device measurements using pixel counting methods:
To farther make sure of the quality of the readings taken with the GRS devices in the field, data was downloaded and analysed in the lab and compared to the original GRS readings taken in the field. Downloading the data was done by connecting the GRS devices up to a computer via USB connection and using the program provided by Radiation Solutions, RSAnalyst. Using the program, it is possible to ask for spectrographs to be saved as bitmap files, which contain the spectrum measured in each assay along with highlighted sections under the spectrum graph showing the areas measured for each of the three elements.

To find the correlation between these highlighted areas and the element concentration measured, the assays completed on the pads at Thebarton were used as they have known concentrations of HPEs. Once this multiplier between the number of pixels highlighted by RSAnalyst and the element concentrations were found, all of the completed assays from Broken Hill and the Reynolds Ranges were downloaded and their pixels counted using Adobe Photoshop to provide a check of the element concentrations provided by the devices in the field. Due to some overlap in gamma emissions between uranium and thorium, the pixel count multiplier found for these two elements was modified to take this into account.

APPENDIX 2: FIGURES OF ELEMENTARY BREAKDOWN OF HEAT PRODUCING ELEMENTS BY METAMORPHIC GRADE (GREENSCHIST TO GRANULITE)

43

Mt Stafford thorium trend, low to high metamorphic grade

Broken Hill thorium trend, low to high metamorphic grade

Reynolds Range thorium trend, low to high metamorphic grade
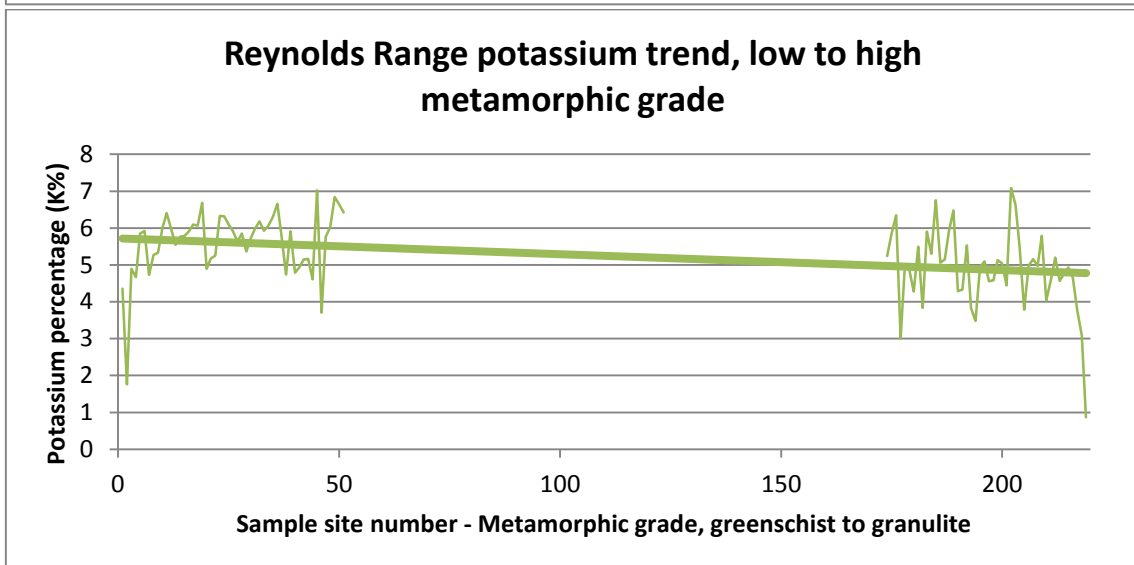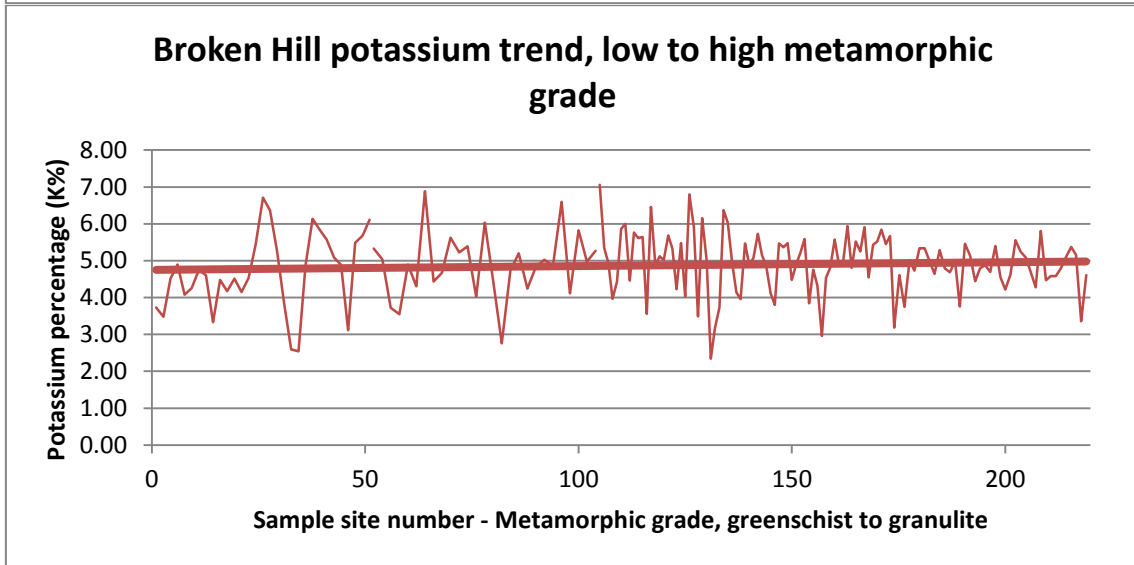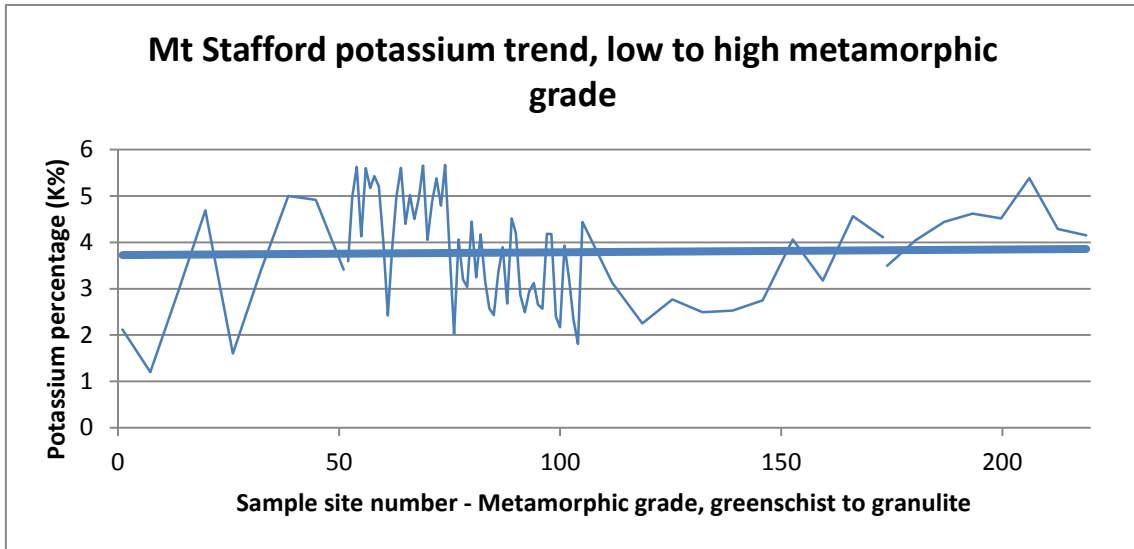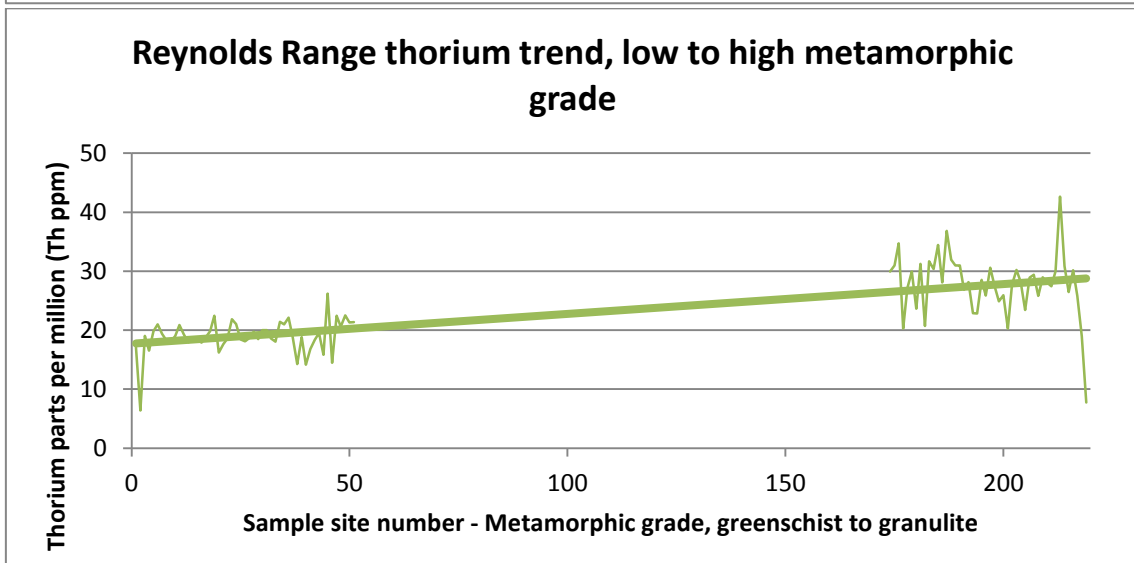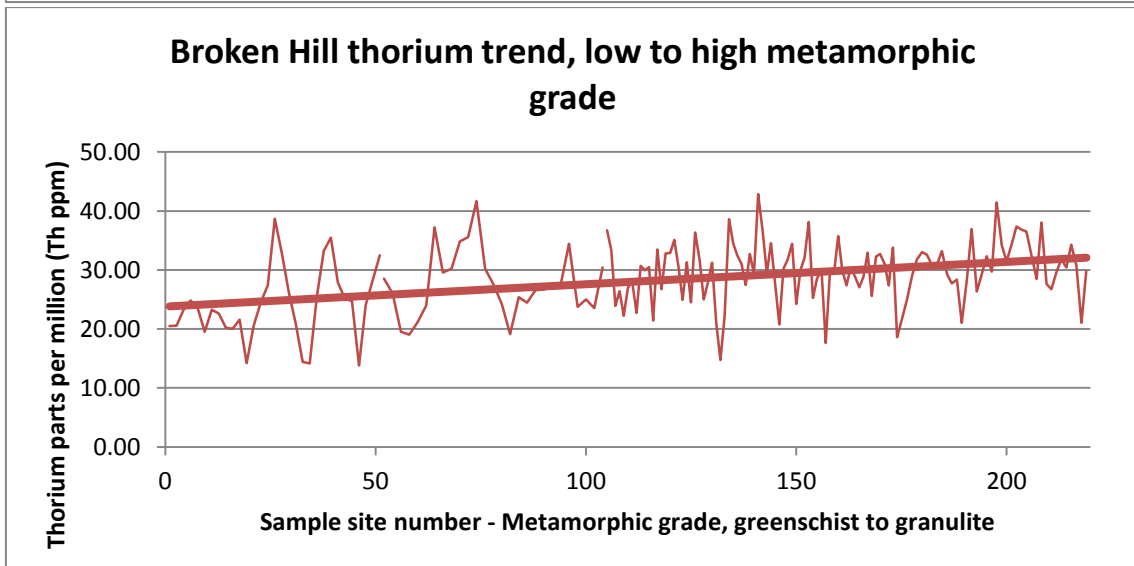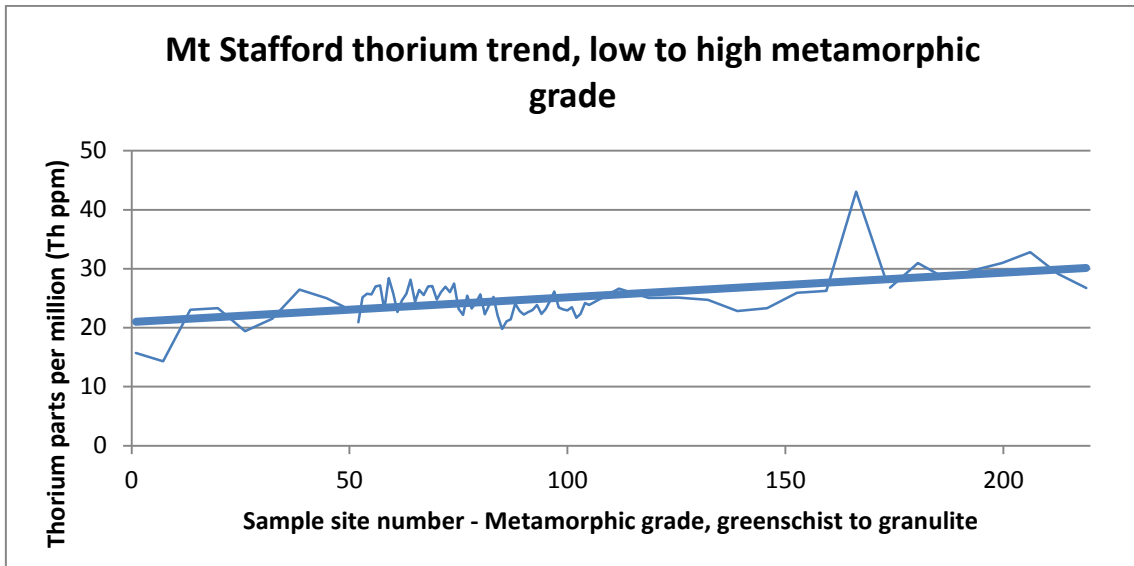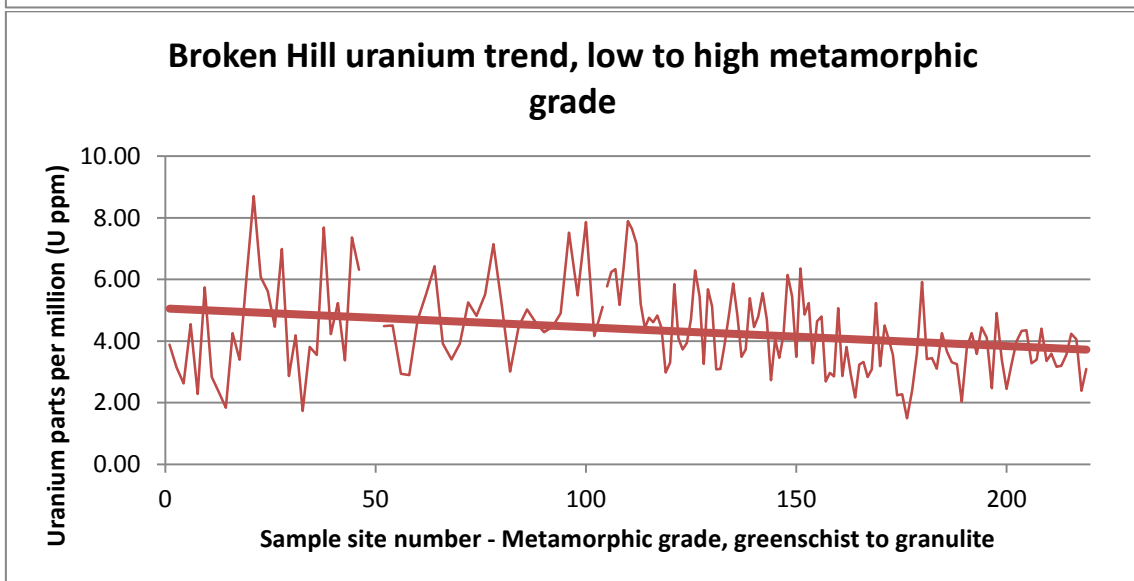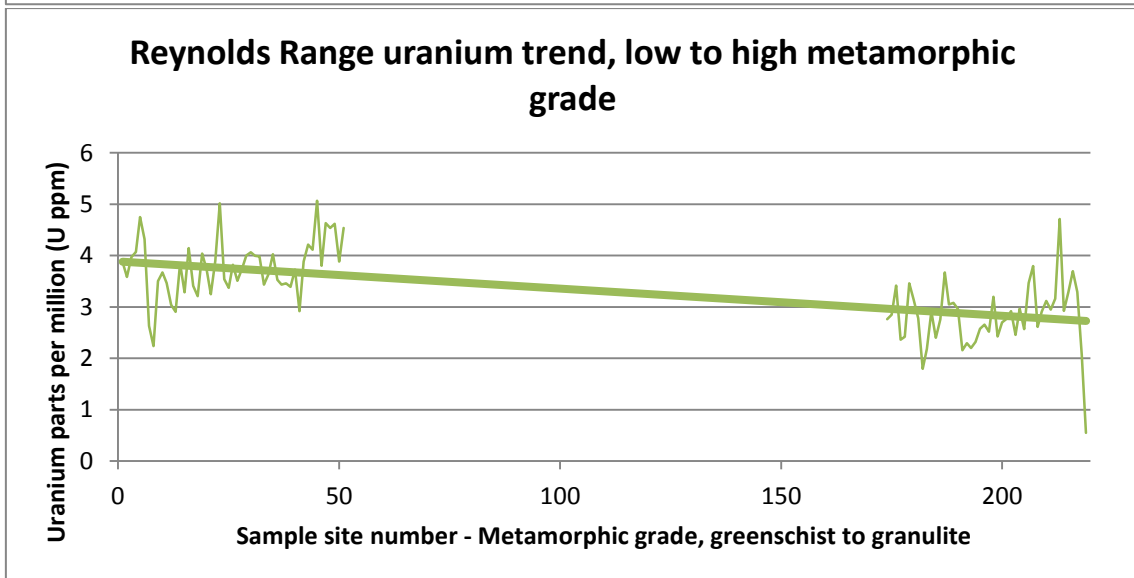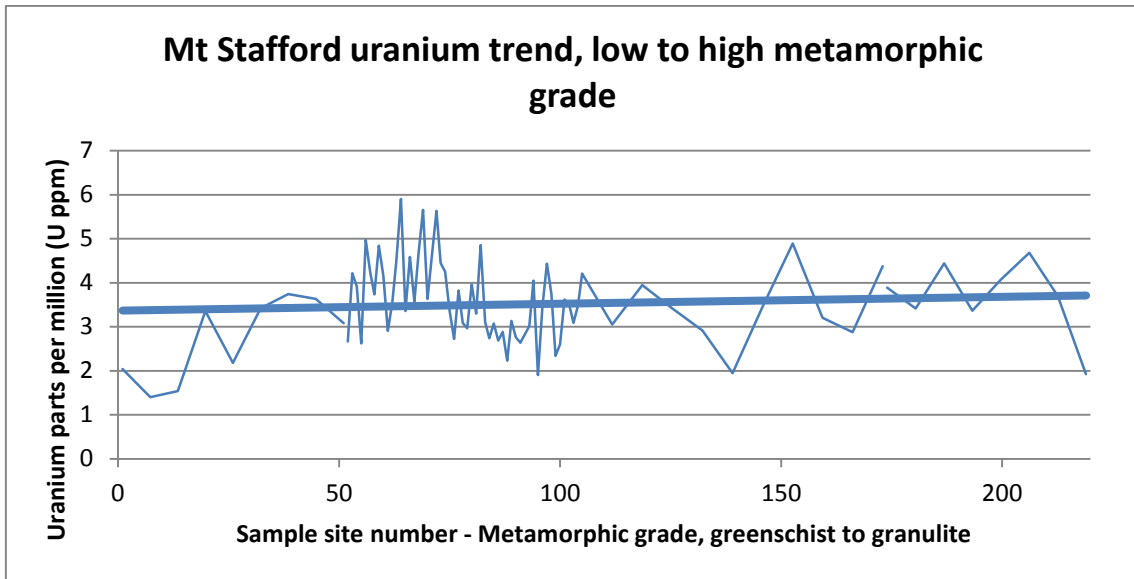
APPENDIX 3: GRS DATA

Mt Stafford Beds:

Zone	Site Number	Southings (53K)	Eastings (53K)	Potassium (K%)	Uranium (U ppm)	Thorium (Th ppm)	RHP (mW/m^3)
Greenshist	84	7562149	246943	2.12	2.05	15.74	1.85
	85	7562135	246947	1.20	1.40	14.32	1.49
	86	7562331	247184	2.92	1.54	23.02	2.30
	87	7562362	247226	4.69	3.36	23.32	2.97
	88	7562484	248127	1.60	2.18	19.39	2.09
	89	7562833	248704	3.38	3.42	21.54	2.74
	90	7561480	250367	5.00	3.75	26.47	3.32
	1	7561484	250329	4.92	3.63	24.98	3.18
	2	7561507	250426	3.41	3.08	22.70	2.73
L Amphibolite	3	7561805	250688	3.59	2.67	20.93	2.51
	4	7562260	251159	4.99	4.22	25.18	3.35
	5	7562275	251144	5.63	3.92	25.74	3.38
	6	7562305	251174	4.13	2.63	25.68	2.89
	7	7562285	251195	5.60	4.97	27.02	3.74
	8	7562300	251251	5.17	4.24	27.19	3.52
	9	7562342	251294	5.43	3.74	23.10	3.12
	10	7562399	251344	5.21	4.84	28.44	3.77
	11	7562416	251355	4.02	4.16	25.80	3.29
	12	7562433	251363	2.42	2.91	22.66	2.59
	13	7562451	251365	3.90	3.55	24.61	3.03
	14	7562488	251374	4.99	4.53	25.76	3.48
	15	7562528	251435	5.61	5.91	28.15	4.07
	16	7562545	251448	4.40	3.36	24.42	3.02
	17	7562573	251477	5.02	4.59	26.44	3.54
	18	7562616	251507	4.51	3.58	25.57	3.17
	19	7562641	251537	4.96	4.67	27.03	3.60
	20	7562651	251553	5.66	5.66	27.09	3.93
	21	7562700	251847	4.05	3.63	24.78	3.08
	22	7562769	251886	4.86	4.64	26.04	3.51
	23	7562821	251910	5.38	5.63	26.94	3.89
	24	7562885	251967	4.80	4.45	26.01	3.45
	25	7562913	252002	5.67	4.26	27.49	3.59
	26	7562935	252078	3.82	3.36	23.22	2.88
	27	7562949	252147	2.02	2.73	22.16	2.47
	28	7563398	251912	4.06	3.83	25.44	3.18
	29	7563443	251963	3.20	3.09	23.25	2.75
	30	7563482	252028	3.04	2.96	24.26	2.77
	31	7563531	252091	4.45	3.96	25.63	3.27
	32	7563599	252103	3.25	3.30	22.28	2.74
	33	7563759	252153	4.17	4.86	23.73	3.34
	34	7563901	252235	3.17	3.11	25.22	2.89
	35	7563982	252277	2.58	2.74	22.09	2.52
	36	7563962	252317	2.43	3.08	19.80	2.43
	38	7563950	252343	3.35	2.69	21.09	2.51
	39	7564072	252341	3.90	2.89	21.44	2.64
	40	7564125	252395	2.68	2.23	24.06	2.53
	41	7564172	252455	4.52	3.13	22.86	2.86
	42	7564194	252568	4.20	2.76	22.22	2.69
	43	7564226	252694	2.87	2.64	22.67	2.56
	44	7564191	252826	2.49	2.83	22.97	2.60
	45	7564136	253033	2.95	3.02	23.84	2.75
	46	7564162	253107	3.12	4.05	22.33	2.93
	47	7564180	253223	2.66	1.91	23.17	2.38
	48	7564365	253564	2.57	3.46	24.57	2.88
	49	7564431	253610	4.18	4.44	26.16	3.40
	50	7564384	253715	4.18	3.75	23.42	3.03
	51	7564385	253835	2.40	2.34	23.09	2.47
	52	7564451	253916	2.17	2.60	22.93	2.50
	53	7564466	253972	3.93	3.62	23.49	2.98
	54	7564515	254022	3.22	3.53	21.67	2.76
	55	7564514	254088	2.33	3.09	22.36	2.61
	56	7564503	254190	1.81	3.48	24.18	2.79

Zone	Site Number	Southings (53K)	Eastings (53K)	Potassium (K%)	Uranium (U ppm)	Thorium (Th ppm)	RHP (mW/m^3)
U Amphibolite	57	7564508	254277	4.44	4.21	23.88	3.21
	58	7564485	254358	3.13	3.06	26.64	2.98
	59	7564485	254463	2.25	3.95	25.04	3.01
	60	7564493	254563	2.77	3.41	25.13	2.93
	61	7564478	254662	2.49	2.92	24.72	2.74
	62	7564483	254750	2.53	1.95	22.81	2.36
	63	7564488	254825	2.75	3.46	23.30	2.81
	64	7564495	254944	4.06	4.89	25.95	3.50
	65	7564496	255020	3.18	3.21	26.26	2.99
	66	7564523	255069	4.56	2.88	43.09	4.22
	67	7565012	254326	4.11	4.38	28.23	3.53
Granulite	83	7563364	259330	3.49	3.89	26.79	3.24
	82	7563405	259431	4.04	3.42	30.97	3.46
	81	7563384	259581	4.44	4.44	28.30	3.58
	80	7563360	259707	4.62	3.37	29.77	3.42
	79	7563357	259858	4.51	4.07	30.98	3.68
	78	7563369	259985	5.38	4.69	32.84	4.05
	77	7563419	260143	4.29	3.70	29.12	3.43
	76	7563409	260253	4.15	1.92	26.76	2.78

Table 3: Mt Stafford Beds GRS data, including sample locations using 53K UTM and individual breakdown of HPEs by sample site.

Sundown Group:

Zone	Site Number	Eastings (54K)	Southings (54K)	Potassium (K%)	Uranium (ppm)	Thorium (ppm)	RHP (mW/m^3)
Yanko Glen	1	550627	6494129	6.11	4.22	32.47	3.98
Greenshist	2	550810	6494217	5.68	11.42	28.33	5.53
	3	550870	6494253	5.48	15.49	24.10	6.28
	4	550979	6494289	3.12	6.32	13.85	2.93
	5	551035	6494305	4.89	7.36	24.71	4.13
	6	551200	6494284	5.09	3.37	25.09	3.14
	7	551345	6494211	5.57	5.24	27.90	3.87
	8	551429	6494230	5.84	4.22	35.48	4.16
	9	551619	6494342	6.13	7.68	33.27	4.94
	10	551661	6494230	4.88	3.55	25.36	3.18
	11	551805	6494099	2.54	3.81	14.14	2.24
	12	551833	6494110	2.60	1.73	14.44	1.72
	13	551914	6494142	3.85	4.19	21.01	2.94
	14	551961	6494162	5.26	2.87	26.12	3.09
	15	551995	6494192	6.36	6.99	32.80	4.75
	16	552082	6494199	6.71	4.47	38.69	4.53
	17	552155	6494194	5.43	5.62	27.37	3.92
	18	552203	6494216	4.53	6.08	24.50	3.75
	19	552681	6494339	4.15	8.70	20.56	4.12
	20	552717	6494344	4.51	6.13	14.22	3.04
	21	552758	6494349	4.18	3.40	21.61	2.81
	22	552831	6494360	4.48	4.26	20.03	2.95
	23	552880	6494360	3.33	1.84	20.20	2.22
	24	552934	6494333	4.60	2.35	22.59	2.65
	25	553069	6494331	4.76	2.84	23.27	2.84
	26	553133	6494360	4.25	5.74	19.55	3.29
	27	553210	6494392	4.08	2.29	23.56	2.65
	28	553261	6494428	4.89	4.55	24.87	3.41
	29	553313	6494436	4.51	2.63	23.25	2.76
	30	553358	6494454	3.48	3.15	20.53	2.60
	31	553456	6494489	3.73	3.88	20.51	2.82
Eldee Creek	33	528904	6494299	5.33	4.49	28.55	3.69
Lower Amphibolite	34	528863	6494347	5.04	4.51	26.05	3.50
	35	528731	6494453	3.72	2.94	19.51	2.50
	36	528689	6494476	3.55	2.90	19.05	2.44
	37	528643	6494540	4.89	4.68	21.14	3.18
	38	528575	6494585	4.30	5.53	23.94	3.55
	39	528442	6494650	6.88	6.43	37.21	4.96
	40	528314	6494674	4.44	3.91	29.58	3.53
	41	528167	6494661	4.67	3.41	30.23	3.47
	42	528021	6494685	5.63	3.92	34.83	4.02
	43	527908	6494644	5.23	5.26	35.59	4.38
	44	527731	6494655	5.39	4.82	41.67	4.71
	45	527640	6494633	4.02	5.51	30.23	3.96
	46	527494	6494516	6.03	7.14	27.53	4.38
	47	527435	6494424	4.46	5.17	24.26	3.49
	48	527401	6494325	2.76	3.01	19.12	2.40
	49	527282	6494305	4.74	4.47	25.38	3.41
	50	527198	6494367	5.20	5.02	24.45	3.53
	51	527185	6494469	4.25	4.62	26.58	3.49
	52	527135	6494547	4.84	4.29	26.70	3.47
	53	527086	6494656	5.03	4.46	27.70	3.60
	54	526955	6494663	4.87	4.91	27.48	3.68
	55	526891	6494620	6.60	7.52	34.47	5.03
	56	526817	6494543	4.12	5.48	23.75	3.50
	57	526788	6494453	5.82	7.86	24.98	4.37
	58	526762	6494351	4.97	4.17	23.54	3.22
	59	526724	6494287	5.27	5.11	30.41	3.98

Zone	Site Number	Eastings (54K)	Southings (54K)	Potassium (K%)	Uranium (ppm)	Thorium (ppm)	RHP (mW/m^3)
Mundi-Mundi Creek	61	523604	6487754	7.06	5.77	36.70	4.77
Upper Amphibolite	62	523588	6487798	5.35	6.24	33.39	4.50
	63	523512	6487893	4.94	6.34	23.94	3.82
	64	523435	6487963	3.97	5.17	26.43	3.59
	65	523469	6488096	4.43	6.42	22.23	3.67
	66	523477	6488189	5.86	7.89	26.97	4.53
	67	523476	6488278	6.00	7.64	28.23	4.56
	68	523488	6488426	4.46	7.16	22.70	3.90
	69	523460	6488571	5.76	5.20	30.69	4.07
	70	523428	6488907	5.61	4.42	29.94	3.80
	71	523162	6488981	5.64	4.76	30.49	3.93
	72	523142	6489053	3.55	4.61	21.41	3.05
Round Hill Traverse	73	548325	6467449	3.19	2.24	18.58	2.20
Granulite	74	548366	6467443	4.61	2.27	21.83	2.57
	75	548386	6467416	3.75	1.50	25.02	2.51
	76	548417	6467381	5.02	2.40	29.10	3.16
	77	548440	6467369	4.73	3.62	31.76	3.64
	78	548462	6467347	5.34	5.92	33.04	4.39
	79	548470	6467325	5.33	3.42	32.62	3.70
	80	548480	6467322	4.97	3.45	30.83	3.55
	81	548495	6467318	4.64	3.11	30.86	3.43
	82	548508	6467310	5.28	4.25	33.19	3.96
	83	548551	6467295	4.79	3.66	29.29	3.48
	84	548574	6467267	4.68	3.31	27.70	3.27
	85	548610	6467268	4.99	3.25	28.35	3.32
	86	548667	6467263	3.76	2.03	21.01	2.37
	87	548690	6467260	5.46	3.81	28.35	3.52
	88	548761	6467205	5.14	4.26	36.91	4.21
	89	548781	6467191	4.45	3.59	26.38	3.22
	90	548808	6467185	4.79	4.44	29.18	3.68
	91	548839	6467182	4.88	4.11	32.34	3.82
	92	548878	6467172	4.70	2.47	29.74	3.19
	93	548910	6467163	5.40	4.92	41.43	4.72
	94	548947	6467153	4.55	3.41	34.20	3.73
	95	548976	6467143	4.21	2.45	31.46	3.26
	96	549006	6467138	4.61	3.27	34.39	3.72
	97	549019	6467141	5.56	3.99	37.37	4.21
	98	549047	6467140	5.24	4.33	36.84	4.23
	99	549065	6467123	5.08	4.35	36.50	4.20
	100	549082	6467116	4.70	3.28	32.44	3.59
	101	549103	6467120	4.28	3.40	28.46	3.30
	102	549115	6467112	5.80	4.40	38.03	4.39
	103	549132	6467120	4.47	3.35	27.61	3.25
	104	549140	6467130	4.58	3.60	26.75	3.26
	105	549161	6467127	4.58	3.17	29.68	3.36
	106	549165	6467110	4.80	3.19	31.80	3.53
	107	549186	6467110	5.10	3.56	30.42	3.56
	108	549201	6467106	5.37	4.24	34.27	4.04
	109	549208	6467117	5.16	4.07	30.82	3.73
	110	549234	6467142	3.36	2.39	21.06	2.43
	111	549289	6467128	4.61	3.10	29.78	3.35

Zone	Site Number	Eastings (54K)	Southings (54K)	Potassium (K%)	Uranium (ppm)	Thorium (ppm)	RHP (mW/m^3)
North East Broken Hill	112	551779	6469818	6.46	4.83	33.45	4.24
Upper Amphibolite	113	551739	6469845	4.86	4.42	26.75	3.51
	114	551691	6469871	5.12	2.98	32.83	3.58
	115	551668	6469885	5.01	3.30	32.89	3.66
	116	551637	6469911	5.68	5.84	35.10	4.55
	117	551596	6469928	5.32	4.10	30.57	3.73
	118	551564	6469954	4.23	3.73	24.94	3.14
	119	551538	6469981	5.48	3.93	31.31	3.76
	120	551512	6469997	4.02	4.71	24.50	3.34
	121	551494	6470009	6.80	6.29	36.37	4.86
	122	551467	6470020	5.93	5.46	31.73	4.23
	123	551439	6470040	3.48	3.26	24.99	2.95
	124	551400	6470069	6.15	5.68	27.86	4.04
	125	551362	6470078	5.01	5.13	31.22	4.02
	126	551341	6470116	2.34	3.08	21.01	2.51
	127	551321	6470147	3.18	3.09	14.75	2.15
	128	551274	6470176	3.73	3.88	22.04	2.93
	129	551219	6470207	6.37	4.88	38.61	4.60
	130	551196	6470227	6.03	5.87	34.51	4.54
	131	551164	6470260	4.92	4.84	32.42	4.02
	132	551097	6470295	4.14	3.49	31.03	3.49
	133	551080	6470301	3.96	3.73	27.47	3.29
	134	551054	6470302	5.47	5.40	32.69	4.24
	135	551028	6470309	4.89	4.45	29.36	3.70
	136	550996	6470330	5.07	4.79	42.87	4.76
	137	550964	6470362	5.72	5.55	36.61	4.58
	138	550929	6470380	5.15	4.71	29.46	3.80
	139	550894	6470399	4.86	2.73	34.56	3.61
	140	550858	6470407	4.11	4.06	27.64	3.40
	141	550821	6470413	3.80	3.45	20.75	2.73
	142	550781	6470409	5.46	4.20	30.19	3.75
	143	550724	6470425	5.37	6.15	31.75	4.36
	144	550702	6470467	5.47	5.45	34.43	4.38
	145	550699	6470492	4.47	3.49	24.23	3.05
	146	550683	6470528	4.92	6.36	29.96	4.24
	147	550659	6470583	5.22	4.86	32.09	4.03
	148	550629	6470615	5.59	5.23	38.15	4.59
	149	550625	6470676	3.85	3.29	25.26	3.01
	150	550596	6470718	4.75	4.64	28.60	3.68
	151	550588	6470762	4.32	4.80	29.90	3.78
	152	550572	6470810	2.96	2.69	17.60	2.23
East Broken Hill	153	555425	6469453	4.54	2.97	29.40	3.28
Upper Amphibolite	154	555453	6469439	4.81	2.85	29.47	3.28
	155	555476	6469424	5.57	5.07	35.73	4.38
	156	555485	6469401	4.91	2.86	29.87	3.32
	157	555513	6469371	4.94	3.81	27.37	3.40
	158	555555	6469373	5.94	2.94	30.39	3.48
	159	555564	6469334	4.80	2.17	28.82	3.06
	160	555580	6469300	5.52	3.24	27.05	3.28
	161	555590	6469279	5.25	3.33	28.84	3.40
	162	555611	6469266	5.91	2.83	32.92	3.63
	163	555621	6469242	4.54	3.09	25.62	3.05
	164	555630	6469219	5.43	5.24	32.28	4.16
	165	555656	6469200	5.52	3.19	32.73	3.67
	166	555687	6469178	5.84	4.51	31.04	3.92
	167	555741	6469135	5.45	4.05	27.37	3.51
	168	555765	6469118	5.67	3.55	33.82	3.85

Table 4: Sundown Group GRS data, including sample locations using 54K UTM and individual breakdown of HPEs by sample site.

Pine Hill Formation:

Zone	Site Number	Southings (53K)	Eastings (53K)	Potassium (K%)	Uranium (U ppm)	Thorium (Th ppm)	RHP (mW/m^3)
Greenshist	1	265475	7541650	4.35	3.89	17.22	2.65
	2	265450	7541640	1.76	3.58	6.41	1.56
	3	265446	7541637	4.89	3.97	19.05	2.85
	4	265435	7541623	4.67	4.07	16.56	2.68
	5	265431	7541601	5.85	4.75	19.86	3.20
	6	265414	7541589	5.92	4.32	20.97	3.17
	7	265395	7541557	4.73	2.63	19.37	2.50
	8	265368	7541551	5.27	2.24	18.23	2.37
	9	265368	7541528	5.32	3.50	18.04	2.70
	10	265307	7541408	6.01	3.67	19.05	2.88
	11	265282	7541371	6.41	3.46	20.89	2.99
	12	265278	7541366	5.98	3.04	19.26	2.72
	13	265265	7541351	5.55	2.90	17.94	2.55
	14	265256	7541339	5.77	3.84	18.32	2.85
	15	265249	7541314	5.79	3.28	18.53	2.72
	16	265243	7541315	5.90	4.14	17.90	2.91
	17	265237	7541293	6.10	3.41	18.75	2.80
	18	265244	7541283	6.07	3.21	19.83	2.82
	19	265244	7541277	6.69	4.04	22.46	3.28
	20	265226	7541256	4.89	3.73	16.19	2.58
	21	265218	7541242	5.17	3.25	17.61	2.58
	22	265219	7541227	5.25	3.90	18.61	2.83
	23	265197	7541223	6.33	5.02	21.87	3.46
	24	265184	7541221	6.32	3.54	21.03	3.01
	25	265186	7541203	6.09	3.37	18.42	2.76
	26	265173	7541191	5.92	3.82	18.08	2.84
	27	265155	7541162	5.64	3.51	18.64	2.77
	28	265144	7541157	5.85	3.73	19.74	2.93
	29	265130	7541138	5.37	4.00	18.50	2.86
	30	265117	7541124	5.73	4.06	20.00	3.02
	31	265097	7541119	5.98	4.00	20.01	3.03
	32	265087	7541103	6.18	3.98	18.59	2.94
	33	265068	7541092	5.93	3.44	18.05	2.74
	34	265057	7541080	6.07	3.64	21.43	3.04
	35	265047	7541056	6.30	4.03	20.98	3.14
	36	265047	7541048	6.65	3.53	22.15	3.12
	37	265012	7541033	5.78	3.43	18.78	2.77
	38	264997	7541011	4.74	3.46	14.26	2.36
	39	264985	7541005	5.91	3.39	18.80	2.78
	40	264979	7540987	4.79	3.73	14.14	2.43
	41	264961	7540974	4.94	2.92	16.79	2.42
	42	264944	7540962	5.15	3.88	18.38	2.80
	43	264925	7540949	5.17	4.21	19.50	2.97
	44	264912	7540924	4.61	4.11	15.82	2.63
	45	265030	7540867	7.02	5.07	26.21	3.84
	46	265068	7540888	3.70	3.80	14.48	2.37
	47	265080	7540900	5.76	4.63	22.47	3.35
	48	265091	7540922	6.03	4.54	20.58	3.21
	49	265121	7540947	6.84	4.62	22.51	3.45
	50	265158	7541014	6.64	3.89	21.30	3.15
	51	265154	7541091	6.42	4.54	21.38	3.31

Zone	Site Number	Southings (53K)	Eastings (53K)	Potassium (K%)	Uranium (U ppm)	Thorium (Th ppm)	RHP (mW/m^3)
Granulite	1	304528	7508062	5.24	2.76	29.93	3.33
	2	304533	7508073	5.86	2.85	30.96	3.49
	3	304543	7508077	6.34	3.42	34.69	3.94
	4	304547	7508096	3.00	2.36	20.29	2.33
	5	304556	7508140	4.94	2.42	27.11	3.01
	6	304562	7508156	4.88	3.46	29.92	3.48
	7	304550	7508162	4.28	3.13	23.65	2.89
	8	304570	7508156	5.49	2.78	31.27	3.45
	9	304550	7508165	3.84	1.80	20.71	2.30
	10	304560	7508177	5.90	2.18	31.66	3.36
	11	304567	7508177	5.30	2.91	30.40	3.41
	12	304566	7508178	6.75	2.40	34.42	3.70
	13	304571	7508189	5.06	2.75	28.11	3.18
	14	304572	7508191	5.15	3.67	36.82	4.05
	15	304575	7508199	5.92	3.05	31.95	3.61
	16	304575	7508197	6.47	3.08	30.99	3.61
	17	304572	7508201	4.28	2.96	30.98	3.37
	18	304581	7508202	4.33	2.16	26.82	2.87
	19	304578	7508210	5.53	2.29	28.12	3.11
	20	304575	7508215	3.83	2.20	22.86	2.55
	21	304586	7508218	3.48	2.32	22.81	2.55
	22	304536	7508220	4.94	2.57	28.51	3.15
	23	304592	7508236	5.10	2.66	25.87	3.00
	24	304603	7508246	4.56	2.52	30.59	3.25
	25	304600	7508256	4.58	3.20	27.40	3.20
	26	304602	7508276	5.13	2.42	24.90	2.88
	27	304600	7508270	5.04	2.70	25.91	3.01
	28	303693	7507963	4.44	2.77	20.29	2.58
	29	303894	7508170	7.08	2.92	27.73	3.39
	30	303900	7508208	6.63	2.46	30.20	3.40
	31	303902	7508213	5.46	2.96	28.18	3.28
	32	303933	7508575	3.78	2.57	23.40	2.68
	33	303935	7508582	4.98	3.47	28.89	3.42
	34	303950	7508608	5.16	3.79	29.42	3.56
	35	303975	7508621	4.97	2.61	25.83	2.98
	36	303935	7508628	5.79	2.91	28.98	3.36
	37	304011	7508644	4.04	3.12	28.10	3.18
	38	304014	7508652	4.57	2.95	27.46	3.14
	39	304031	7508650	5.20	3.16	30.00	3.44
	40	304039	7508656	4.56	4.71	42.65	4.67
	41	304045	7508666	4.75	2.92	30.88	3.39
	42	304060	7508679	4.93	3.29	26.46	3.19
	43	304073	7508682	4.66	3.70	30.17	3.54
	44	304084	7508688	3.76	3.29	25.80	3.04

Table 5: Pine Hill Formation GRS data, including sample locations using 53K UTM and individual breakdown of HPEs by sample site

APPENDIX 4: XRF GEOCHEMICAL DATA

Mt Stafford Beds:

Grade	Sample (STF)	Southings (53K)	Eastings (53K)	Yttrium (ppm)	Zirconium (ppm)	Lanthanum (ppm)	Cerium (ppm)	Uranium (ppm)	Thorium (ppm)	RHP (mW/m³)
Greenshist	31a	7562149	246943	21.5	222	35	63	4.9	34	3.59876
	31b	7562149	246943	37.5	273	55	104	2.4	48	4.76256
	32	7562331	247184	9.9	340	30	100	0.9	36.9	3.59469
	33	7562362	247226	22.2	224	43	75	0.7	27.2	2.65232
Lower Amphibolite	1	7562275	251144	23.4	85	41	106	0.25	39	3.7499
	3	7562285	251195	23.1	200	39	70	0.7	26.8	2.61404
	4a	7562300	251251	24.7	335	46	80	3.2	37	3.76618
	5	7562342	251294	28.2	102	42	106	0.25	35.1	3.37667
	7	7562913	252002	28.6	151	45	112	1.5	30.3	3.00531
	9	7563491	252042	37.0	101	48	140	5	33	3.5101
	16b	7564418	252677	28.5	92	42	109	0.25	29.6	2.85032
	17a	7564418	252677	15.9	235	37	73	0.6	30.5	2.96109
	17b	7564418	252677	16.7	200	31	69	0.5	28	2.7148
	18	7564417	253577	16.5	95	33	76	0.25	22.5	2.17085
Upper Amphibolite	21a	7565037	254335	20.4	234	39	64	1.3	29.1	2.87639
	21b	7565037	254335	20.0	213	34	69	2.6	36.6	3.68566
	21c	7565037	254335	24.1	128	37	78	1.6	31.8	3.1559
	20	7565053	254680	18.7	349	38	83	1.3	38.8	3.80468
Granulite	28	7563459	260116	31.7	178	50	111	1.2	48	4.67808
	29	7562150	246946	18.9	326	43	79	0.5	23.7	2.30329
	30	7563436	260031	38.3	84	46	101	1.1	34	3.33124
	26	7563397	260269	25.3	206	39	73	0.25	25.3	2.43881
	27	7563459	260230	19.1	340	39	79	1.6	31.9	3.16547

Table 6: Mt Stafford Beds geochemical samples, including sample location and metamorphic grade.

Pine Hill Formation:

	Sample	Southings (53K)	Eastings (53K)	Yittrium (Y ppm)	Zirconium (Zr ppm)	Lanthanum (La ppm)	Cerium (Ce ppm)	Uranium (U ppm)	Thorium (Th ppm)	RHP (mW/m3)
Greenschist	RR2014-1A	7540867	265030	36.1	290	56	128	1.3	32.0	2.59314
	RR2014-1B	7540867	265030	32.7	284	56	117	0.7	30.0	2.29526
	RR2014-1C	7540867	265030	32.1	282	56	120	0.9	31.0	2.41802
	RR2014-2A	7540900	265080	28.6	173	45	100	1.9	31.0	2.67982
	RR2014-2b	7540900	265080	31.5	176	48	120	0.8	31.0	2.39184
	RR2014-2c	7540900	265080	31.0	185	41	93	<0.5	34.0	2.3936
	RR2014-2d	7540900	265080	30.8	193	43	101	0.5	36.0	2.6653
	RR2-14-3a1	7540900	265080	24.0	135	26	53	<0.5	26.0	1.8304
	RR2014-3a2	7540900	265080	26.8	131	24	51	<0.5	27.0	1.9008
	RR2014-3b	7540900	265080	25.5	134	26	52	<0.5	22.0	1.5488
	RR2014-3c	7540900	265080	24.3	127	26	52	<0.5	25.0	1.76
	RR2014-4a	7540947	265121	15.5	211	37	77	<0.5	26.0	1.8304
	RR2014-4b	7540947	265121	15.3	192	36	69	<0.5	26.0	1.8304
	RR2014-4c	7540947	265121	15.9	208	38	103	<0.5	25.0	1.76
	RR2014-4d	7540947	265121	15.0	184	35	47	<0.5	26.0	1.8304
	RR2014-5a	7541091	265154	17.5	193	46	93	0.6	27.6	2.10012
	RR2014-5b	7541091	265154	18.4	191	42	89	0.5	33.0	2.4541
	RR2014-5c	7541091	265154	16.5	188	42	98	1.0	27.5	2.1978
	RR2014-5d	7541091	265154	17.7	189	43	93	<0.5	28.4	1.99936
Granulite	RR2014-6a	7508270	304600	32.8	236	36	88	<0.5	36.9	2.59776
	RR2014-6b	7508270	304600	30.1	219	36	84	1.2	36.7	2.89784
	RR2014-6c	7508270	304600	24.6	236	32	72	1.4	36.1	2.90796
	RR2014-7a	7508199	304575	17.2	496	38	74	1.2	44.3	3.43288
	RR2014-7b	7508199	304575	11.7	565	33	62	2.7	33.5	3.06526
	RR2014-7c	7508199	304575	14.7	768	36	61	0.9	37.5	2.87562
	RR2014-8a	7508162	304556	18.3	478	38	73	1.7	44.1	3.5497
	RR2014-8b	7508162	304556	20.0	430	37	65	1.2	32.3	2.58808
	RR2014-8c	7508162	304556	17.3	414	34	73	<0.5	38.2	2.68928
	RR2014-8d	7508162	304556	15.3	452	35	67	<0.5	35.5	2.4992
	RR2014-9a	7508140	304556	2.7	325	20	34	<0.5	15.2	1.07008
	RR2014-9b	7508140	304556	3.0	329	16	31	<0.5	24.1	1.69664
	RR2014-9c	7508140	304556	3.4	306	19	39	<0.5	22.9	1.61216
	RR2014-10a	7508077	304543	22.7	120	8	49	4.8	36.0	3.79104
	RR2014-10b	7508077	304543	26.2	120	7	40	4.8	33.9	3.6432
	RR2014-10c	7508077	304543	24.3	125	8	44	7.4	45.3	5.12644
	RR2014-11b	7508062	304528	23.0	335	33	60	1.1	32.1	2.54782
	RR2014-11c	7508062	304528	17.8	325	29	57	0.5	27.6	2.07394

Table 7: Pine Hill Formation geochemical samples, including sample location and metamorphic grade